MAPPING PROBABILITIES OF ARABLE FIELDS USING MODIS, SENTINEL-1 AND SENTINEL-2 BASED IMAGE FEATURES IN GHANA

MANUSHI BHARGAV TRIVEDI
July, 2020

SUPERVISORS:
Dr. M.T. Marshall
Dr.ir. C.A.J.M. de Bie

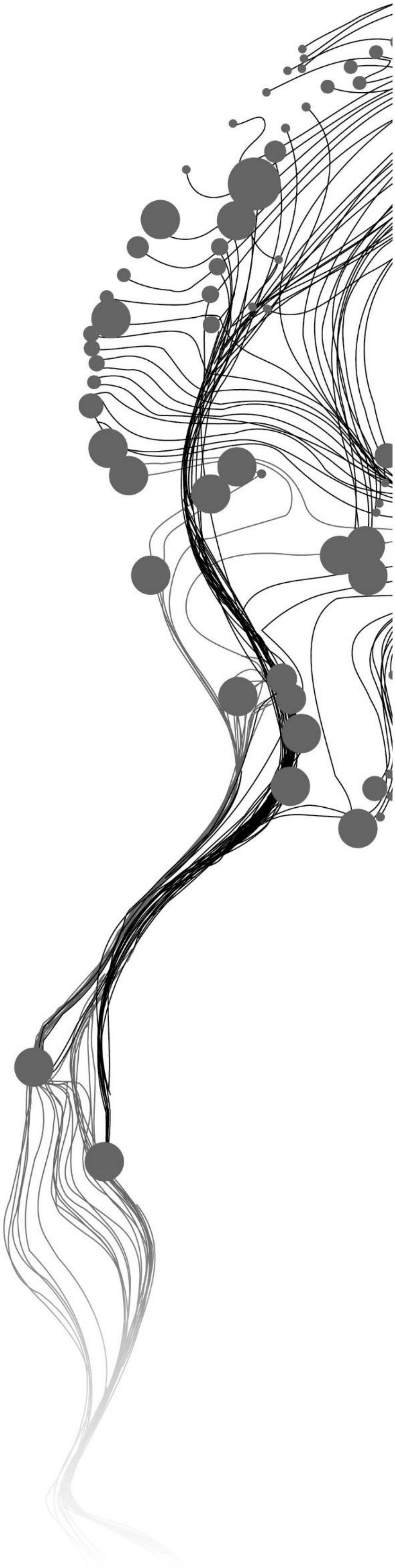

MAPPING PROBABILITIES OF ARABLE FIELDS USING MODIS, SENTINEL-1 AND SENTINEL-2 BASED IMAGE FEATURES IN GHANA

MANUSHI BHARGAV TRIVEDI
Enschede, The Netherlands, July, 2020

Thesis submitted to the Faculty of Geo-Information Science and Earth Observation of the University of Twente in partial fulfilment of the requirements for the degree of Master of Science in Geo-information Science and Earth Observation.
Specialization: Natural Resources Management

SUPERVISORS:
Dr. M.T. Marshall
Dr.ir. C.A.J.M. de Bie

THESIS ASSESSMENT BOARD:
Prof. Dr. A. D. Nelson
Dr. Lyndon Estates (External Examiner, Clark University)

Dedicated to Pappa………

ABSTRACT

To cope up with the current demand and supply chains of agricultural products, monitoring the food production capacity via the national or regional level agricultural database on forecasted crop productions is necessary. The location and extent of cultivated cropped area is the critical input for mapping precise crop yields. Current remote sensing methods addressing the combined use of the open-source satellite data are very few and are efficient for northern countries but cannot be adopted where Arable Fields Area (AFA) is typically characterized as irregularly shaped and difficult to distinguish. Recent remote sensing-based available global land cover products are inconsistent across the globe. They do not address the complexity of agriculture landscapes, and it majorly focuses on the use of high or very high spatial resolution images (<5m).

Hence, this research has focused on identifying the potential of freely available earth observation data based satellite image features for estimating probabilities of AFA in the African agricultural landscape (Eastern region in Ghana as a case study). Higher temporal MODIS images are used for capturing long-term vegetation climatology pattern to stratify the landscape. Based on which dry and wet seasons and strata with cropping intensity via Crop Productive Zones (CPZs) on the regional level has been derived. It has addressed the landscape heterogeneity at the pixel level via homogenous stratification. The use of the median composite of Sentinel-1 (S1) and Sentinel-2 (S2) images across the dry and wet seasons and, over the years (2017-2019), is exploited due to its spatial, temporal, spectral, and polarimetric capability to differentiate AFA with other vegetated and non-vegetated areas. In lines with it, topographical and textural image features are also examined for explaining additional local and regional level arable field distribution. In this study, one temporal (CPZs), two topographic (Slope and Elevation), 14 spectral (optical and red-edge vegetation indices), ten polarimetric (Dry and Wet VV, VH, VV/VH, VV+VH, VV-VH) and 110 texture (Dry and Wet S1 & S2 variance, homogeneity, dissimilarities, entropy, contrast) image features have been studied extensively. The relevant image features have been identified for mapping AFA and its probabilities have been mapped using the RandomForest (RF) algorithm.

A total of 36 important features have been selected, out of which 33 features are texture features (majorly Variance texture), one is topographic (Elevation), one is temporal (CPZs), and one is polarimetric (Dry VV) image feature. Where topographic and texture features, in general, improve prediction by reducing 0.14 to 0.10%, temporal CPZs feature reduces 0.05%, and polarimetric feature reduces 0.04% error in Brier Score (BS). In general, the topographic elevation and, optical and radar-based texture feature outperformed the spectral features. It also outperformed a temporal and polarimetric image features in a way as well. It is also important to note that the challenge of extreme cloud cover in optical images have been addressed via the median composite of the images over long-term (three years) (2017-2019) and seasonal changes (different dry and wet period) for the different region within the study area have been identified and implemented well. However, the performance of RF for predicting the extremes probabilities is skeptical or leveraged at extreme points, and it needs further improvement via the change in sampling design and image processing (especially image integration).

Keywords: Sentinel-1, Sentinel-2, MODIS, SRTM, Texture, Topography, Temporal, Spectral, Polarimetric, Arable field area

ACKNOWLEDGMENTS

I would like to thank dr. Michael Marshall, for constant supervision, care, and backbone idea behind the research conducted in the thesis. Not only during the research but also from early coursework at ITC, he has been there for guidance. He also introduced me to a great opportunity of internship inlined with research, which has broadened my horizons of understanding. During the research work as well, we have explored different angles of research and had fruitful insights. Not only as a student-teacher but also as a friend, he has supported me in my hard and good times, for which I am very grateful to him, and I hope we will share more in the future.

I would like to thank dr. Kees de Bie as well, as he has been mentoring me not only in past months but from the start of the ITC coursework. He has helped me to develop critical thinking and helped me to learn 'seeing and believing.' He introduced me to time component in satellite imagery with a very different perspective, for which I will always be grateful. He has explained all of my questions with patience at all times, and I have always appreciated it.

During the research time, I have been involved in an internship at Clark Labs, where I have met dr. Lyndon Estates. He introduced me to different new and advanced perspectives of work in the geospatial industry and has taken great care of my well being during the internship. I have learned to handle multiple things efficiently, which I will surely follow in the future.

I would also like to thank faculties with whom I have been encountered since my first day at ITC for creative learnings they have offered. I thank not only faculties but also to my family and friends for being there as emotional support.

TABLE OF CONTENTS

LIST OF FIGURES

LIST OF TABLES

1. INTRODUCTION

1.1. Background and motivation

The world is facing a continuous rise in global hunger due to the increasing global population, which puts pressure on the current global food production capacity and demands it to be double in the future. Not only day by day increasing population, but also the recent climatic variabilities like changes in rainfall pattern, its distribution, seasons, temperature make it even harder to reach out to the global food security targets (FAO, IFAD, UNICEF, 2018). Moreover, as per the equation *Farm Production = Crop yield x Crop acreage*, the location and extent of cultivated cropped area is the critical input to ultimately map precise yields and help decision-makers to prevent the threats related to food production (FAO, 2003; Kahubire, 2002). Therefore, to cope up with the current demand and supply chains of agricultural products, monitoring the food production capacity via the national or regional level agricultural database on forecasted crop productions is necessary. Also, for better monitoring of the current food production system and capacity, information on crop yields, cultivated areas, and their locations are key elements to locate the agricultural risk involved due to climate change. It can also be used for early warnings in food production monitoring systems, for example, FAO Global Information and Early Warning System (GIEWS), Global Monitoring for Food Security (GMFS) (Waldner, Fritz, Di Gregorio, & Defourny, 2015). Global crop extent maps can not only be helpful for food security but also be considered as added value for climate models, understanding crop behaviors for various agro-systems, its impact on the environment, hydrological models, international trade, etc. (Hannerz & Lotsch, 2008).

Zooming to sub-Saharan Africa, mapping the crop extent is very important as agriculture holds major shares in development (Hannerz & Lotsch, 2008; Vancutsem, Marinho, Kayitakire, See, & Fritz, 2012). Specifically, countries like Ghana, where the majority share is of rain-fed agriculture, and 90% of its cultivated lands under smallholder farms (Ministry of Food and Agriculture, 2011) adds in the risk related to climate change. These rainfed subsistence agriculture areas are highly affected by the variability of spatial-temporal rainfall distribution due to frequent climatic extremes in past years (Connolly-Boutin & Smit, 2016). Crop location information for countries like Ghana is crucial where the share of agriculture in Gross Domestic Product (GDP) has been consistently more than 21% from 2013 to 2017 (Ghana Statistical Service, 2019) yet difficult to collect this information due to complex geography. The conventional way to collect information about the annual crop area is agricultural surveys or censuses carried out by agriculture extension officers, which have most likely data quality challenges (The World Bank, 2017). The challenges are mostly because of inconsistent on-ground surveying methods, and biennial or mixed cropping patterns followed in the fragmented landscape. Annual surveys are also cost and labor-intensive; moreover, surveys based crop area information is in tabular form, which is incompatible due to its limitation of locating farms at a detailed spatial scale and various temporal scale (Kahubire, 2002). To overcome these social or on-ground problems, remote sensing-based earth observation imageries provide consistent, efficient, affordable, and reliable information for large scale mapping of the agriculture areas (Atzberger, 2013).

Earth observation-based satellite images contain information at multiple spatial (very high or high : <5m, moderate: 10-30m, lower: >100m), temporal (high: 1-5 days, moderate: 15-30 days), and spectral resolutions. Higher-temporal images capture the seasonal and interannual variations of crop fields due to its high revisit frequency (1-5 days) in time and long term (more than 15 years) availability at a coarser spatial resolution. Freely available images like Moderate Resolution Imaging Spectroradiometer (MODIS), provide long records from 2000 to present in visible (VIS), Near-Infrared (NIR), Shortwave Infrared (SWIR), and Thermal Infrared (TIR) bands, which helps to analyze climatic behavior of vegetation over the years. These long-term time-series based temporal profiles can be summarized on an annual basis via median or mean. Due to MODIS' frequent and longer cloud-free records smooth annual temporal profiles can be achieved and further used to stratify heterogeneous landscape into homogenous strata with common attributes shared (Khan, de Bie, van Keulen, Smaling, & Real, 2010; Mohammed, Marshall, de Bie, Estes, & Nelson, 2020). Based on these strata vegetation types like the forest, agriculture, natural vegetation can be differentiated by identifying changes in temporal profiles. For example, forest areas will have marginal variation throughout the years compared to agriculture areas with a distinct increase and decrease in temporal satellite records as per cropping seasons (Khan et al., 2010; Mohammed et al., 2020). Long-term climatology temporal pattern can be used not only for stratification of landcover types but also be used to stratify within agriculture types via stratified Crop Productivity Zones (CPZs) or agro-ecological zones for a given landscape. It gives insights about cropping seasonality, frequency, and type at the landscape level (Khan et al., 2010). For example, arable agriculture with different cropping intensity expressed in the percentage of cropped area at coarser spatial resolution can be calculated via disseminating the district level crop area statistics. However, it fails to accurately map the 1 ha (100 x 100m) fields or small fields due to lower spatial resolution (L.D. Estes et al., 2016).

Higher Spatial (HS) resolution images capture detailed spatial variation, which is very useful for accurate crop area demarcation but has a lower revisit time. Moreover, HS resolution images have higher heterogeneous but merely similar pixels that impede the modeling process. On the other hand, the stratification of landscape reduces the complexity in the images by homogenous strata. An open-source mission like Sentinel-2 (S2) (A+B) by European Space Agency (ESA) captures optical passive sensor based images at 10m to 20m with a temporal resolution of 5 days interval from 2017 to present and are very useful in delineating the field's area (Watkins & Niekerk, 2019). S2 images also provide additional spectral information compared to Landsat's mission via narrow Red Edge (RE) bands at 700nm, which is sensitive to chlorophyll and nitrogen content in the plant canopy (Clevers & Gitelson, 2013). Due to its sensitivity to plant canopy content, it helps to differentiate agriculture vs. other types of vegetation as arable fields have higher nitrogen and chlorophyll content compared to natural vegetation. However, single date optical satellite sensors based image has limitations because of optical sensors' incapability of penetration through the clouds due to shorter wavelengths resulting in cloudy images during the crop growth cycle. The impact of clouds can be reduced using a median composite or averaging long-term (3-5 years) images over the dry and wet season which also shows the distinct difference in the wet and dry season for arable agriculture area than other landcover types (Debats, Luo, Estes, Fuchs, & Caylor, 2016; Mohammed et al., 2020). Although compared to Landsat's mission, S2 has a higher temporal resolution, which indicates the higher potential of S2 cloud-free images over the seasons.

Microwave active sensor-based radar (Radio Detection and Ranging) images provide accurate and timely updates on ground measurements due to the capability of the longer wavelength to penetrate through clouds compared to optical sensor based shorter wavelength (N. D. Herold, Haack, & Solomon, 2005). Sentinel-1 (S1) (A+B) mission of ESA based freely available radar images are useful to capture crop phenological changes accurately in dry and wet seasons due to cloud-free data. These Synthetic Aperture Radar (SAR) images contain information about backscattered energy from the earth's surface feature, which is characterized by phase and amplitude. The reflected backscatter value is sensitive to canopy moisture content, volume, and roughness, as well as sensor view angle, and topography (Tadesse &

Falconer, 2014). Besides, S1's backscattered energy in dual-polarization (Vertical and Horizontal) has a strong correlation with growing crop biophysical properties due to its sensitivity of surface and volume scattering (Abdikan, Sekertekin, Ustunern, Balik Sanli, & Nasirzadehdizaji, 2018). Vertical transmit and Vertical receiver (VV) polarization is useful for mapping crop height, and Vertical transmits and Horizontal receiver (VH) are useful for mapping crop canopy structure. The use of radar images requires expert skills in terms of processing and visual interpretation (N. D. Herold et al., 2005). Moreover, due to noisy data and recent data acquisition, it is still a less explored area (Xu, Zhang, Wang, Zhang, & Liu, 2018).

Topographic and texture information derived from open-source Earth observation data adds in the value for crop mapping by considering the topography expressing field distribution and texture expressing additional spatial dependencies and variation in neighborhood pixels (Recio, Hermosilla, Ruiz, & Fernández-Sarría, 2010). Shuttle Radar Topography Mission (SRTM) based Digital Elevation Model (DEM) image by National Aeronautics and Space Administration (NASA) at 30m resolution provides topographical information like elevation from above sea level, from which, the slope can also be derived. For mapping, the fields, topographic can play a crucial role as it explains the distribution of the fields in the landscape (Marshall et al., 2011).

Textural images can also be significant for agriculture fields mapping, as it gives an idea of the spatial distribution of pixel intensity values in the surrounded pixels (Debats et al., 2016b). One of the most frequent techniques like Grey-Level Co-Occurrence Matrix (GLCM) based image textures, give an idea about canopy's structural component and its arrangement. For example, crop canopy will have relatively lower contrast, dissimilarity, and high homogeneity within the fields than the forest canopy (Haralick, Dinstein, & Shanmugam, 1973).

Not only the data characteristics but also classification techniques influence the mapping accuracy. The small and large arable fields can be mapped using manual digitization using very high spatial resolution images, although, its time consuming, subjective and inefficient due to land cover dynamics (Tokarczyk, Wegner, Walk, & Schindler, 2015). As an alternative, pixel-based supervised classification, which uses field observations as a training sample (Mohammed, 2019), and unsupervised classification, which is based on error function (Enderle & Weih, 2005), has been used to assign each pixel under one land cover class category. Unsupervised classification models like ISODATA clustering, K-nearest neighbor are useful to apply in the unknown area as it does not require prior knowledge of study area and creates homogenous clusters, despite that, it is time-consuming to assign the labels to these clusters afterward (Xiong, Thenkabail, Gumma, et al., 2017). The machine learning-based non-parametric algorithms like Random Forest (RF) have been used as supervised classification techniques as it is more efficient. Unlike the statistical model, it does not assume the pre-distribution data patterns (Rogan, Chen, & Rogan, 2004), and it can also handle large multiple feature datasets and noise (Belgiu & Drăgu, 2016).

In a way, remote sensing-based different types of satellite image features are helpful for crop field mapping. Higher-temporal images capture climatology of the vegetation, although its limitation of coarser spatial resolution can be addressed via HS resolution of S1 and S2 images with multi-spectral data. Not only S1 and S2 based cloud-free spectral and polarimetric image features, but also topographic and texture image features provide advanced information for mapping various vegetation types and their distribution. However, current RS methods addressing the use of these open-source data together are rare, or none and the majority focused on northern countries using few image features. Still, it cannot be adopted where Arable Fields Area (AFA) is typically characterized as irregularly shaped and difficult to distinguish because of fragmentation in sub-Saharan-Africa (Debats, Luo, Estes, Fuchs, & Caylor, 2016a). Not only clouds and characteristics of AFA, but landscape heterogeneity also cause spectral, spatial, and temporal overlap with natural vegetation leads to an overestimation of mapped AFA. Due to the fragmented landscape, identifying AFA at moderate spatial resolution (30m) and separating it from natural vegetation at moderate spectral resolution can be difficult. Also, weeds and other natural vegetation show temporal variation during rainy seasons at a finer spatial scale, especially in rain-fed agriculture, which can be resulted in the false mapping of AFA.

1.2. Problem Statement

Remote sensing-based currently available global land cover products are inconsistent across the globe. They do not address the complexity of agriculture landscapes like field distribution, cropping pattern & seasonality, cloud cover during the growing season, spectral similarities with natural vegetation, which are important considerations for crop area mapping (Waldner et al., 2015). Especially the use of these crop area maps is limited in sub-Saharan Africa due to small and irregularly shaped fields. Yet, it is very important as the food production per capita is declining, and the population keeps increasing rapidly in sub-Saharan Africa compared to the world (Brown, Funk, Galu, & Choularton, 2007). In the proposed study, only arable agriculture or Arable Field Area (AFA) has been focused on mapping. AFA is defined by the Food and Agriculture Organization(FAO), as, "land under temporary crops (double-cropped areas are counted only once) or temporary meadows for mowing or pasture" and modified for this study as per "land under temporary crops (double-cropped areas are counted only once) or temporary meadows for mowing or pasture which have sowing and harvesting cropping season in past three years". Therefore, tree crops like cocoa and oil palm present in the landscapes are not focused to map.
AFA can be mapped accurately in geographically complex regions by human pattern recognition based crow-source platform and very high spatial (VHS) resolution optical (PlanetScope (PS), world-view; <5m) images due to its ability to distinguish small fields (L.D. Estes et al., 2016). Although, processing of VHR images is time and cost consuming. Due to the higher costs, it has limited usage for researchers in Africa. Additionally, many remote sensing methods focus on the sub-pixel approach for mapping crop areas using VHS resolution images, which may not be efficient in West African AFA (Vintrou et al., 2012).
On the other hand, individual open-source satellite data have their advantage and disadvantage for AFA mapping, but it can be used together for accurate mapping of AFA. For example, open-source satellite images like S2, have relatively moderate spatial & temporal resolution, which can help to map AFA with minimal cost. Despite that, due to west African monsoon, countries like Ghana have continuous cloudy weather during the whole year (Lohou et al., 2014), resulting in limited available cloud-free images in the growing season, which challenge the use of only S2 images. To overcome the clouds, S1 radar images capture the crop phenology in both growing and off-growing seasons due to penetration capabilities through clouds & sensitivity towards crop growth volume, which can be used as a valuable source for AFA mapping. Moreover, topographic open-source satellite image features are also likely to improve mapping AFA due to complex terrain and field distribution in the landscape (Marshall et al., 2011b). Concerning landscape organization, classical raw image bands do not make sufficient use of spatial concepts of the neighborhood, proximity, or homogeneity in surrounded pixels (Burnett and Blaschke, 2003). Several authors used texture analysis to classify VHS resolution images for crop area mapping (e.g., Kayitakire et al., 2006; Peddle and Franklin, 1991), but very few studied possibilities of using the texture of moderate spatial resolution (10-30m) images in landcover classification (see Tsaneva et al. (2010) for one example). In a way, very few studies have focused on using one or two of these open-source image features to map AFA in West Africa, where areas have persistent cloud cover and fragmented landscape.

1.3. Research Objectives and Questions

Hence, this research proposed to identify relevant image features and, to develop an accurate and robust method to estimate AFA with freely available Earth observation data for the African agricultural landscape. For which, higher temporal MODIS images are used capturing long-term vegetation climatology pattern, to stratify landscape, based on which dry and wet seasons and strata with cropping intensity via CPZs on the regional level have been derived. The use of the median composite of S1and S2 images across three years (2017-2019) and two seasons (dry and wet seasons) are exploited due to its spatial, spectral, and polarimetric capability to differentiate AFA with other vegetated and non-vegetated areas. In lines with it, topographical slope and elevation and textural image features are also examined for explaining additional local and regional level arable field distribution.

Based on the above discussion and reasoning, the main research aim of the proposed study is to identify most discriminate satellite image features for mapping AFA and to map AFA probabilities using RandomForest (RF) multi-source freely available earth observation satellite-based image features as mapping predictors at 30m in the fragmented agriculture landscape of Eastern region, Ghana. The detailed objectives and research questions of the study areas discussed below:

1. To identify dry and wet vegetation seasons for NDVI strata based on frequent and longer-temporal MODIS images based landscape stratification from 2003 to 2009
2. To evaluate the performance of CPZs as temporal features based on frequent and longer-temporal MODIS images based landscape stratification for estimating AFA probabilities
    a. To what degree higher-temporal 250m MODIS Terra+Aqua NDVI images base stratified homogenous CPZs improve the estimation of AFA?
3. To evaluate the performance of S1 radar images and S2 optical images based polarimetric, spectral and textural features for estimating the AFA probabilities
    a. To what degree S1 based polarimetric (VV, VH) image features improve the estimation of AFA significantly?
    b. To what degree S2 based spectral image (optical and red-edge vegetation indices) features to improve the estimation of AFA significantly?
    c. To what degree S1 & S2 based texture image (Variance, Contrast, Homogeneity, Dissimilarity, Entropy) features improve the estimation of AFA significantly?
4. To evaluate the performance of SRTM based DEM and slope as topographical image features for estimating the AFA probabilities
    a. To what degree topographic SRTM (Elevation, Slope) based image feature significantly improves the probabilities of AFA mapping?

2. RELATED WORK

2.1. Remotely sensed higher-temporal NDVI time series & CPZs

Rather than raw bands, vegetation indices (VI) like Normalized Difference Vegetation Index (NDVI), which is the ratio of red and NIR bands, is more sensitive to vegetation due to the plant chlorophyll content (Geerken, Zaitchik, & Evans, 2005) and less sensitive to soil background, topography and atmosphere. Based on these long-term temporal profiles, cropping intensity based on annual seasonality like monomodal, bimodal, or multimodal can also be identified and effectively used to characterize location or area-specific dry and wet seasons. To delineate the seasonality from the temporal profiles, Reed (1994), has found the simple and quick method to characterize the seasons by moving the average model with an ideal four months window size. The same techniques have been widely used in west-Africa for seasonal characterization (Mohammed et al., 2020).

Based on these annual dry and wet seasons, long-term mean dry and wet images can be synthesized. Khan et al. (2010) in Spain & Ali (2014) in Ghana found a further correlation between these annual vegetation temporal profiles and government surveyed crop area statistics to stratify CPZs in terms of % probabilities of cropped area per each pixel. In a way, these CPZs show the cropping intensity per pixel and can also help to identify the type of crops. Mohammed (2019) used this % of crop area probabilities as a categorical predictor to classify the crop area probabilities at 30m using Landsat 8 data, and it is found that these coarser-resolution based field fractions explain the majority deviance in a geographically complex region of Ethiopia. He also concluded that extracting temporal features like long-term averaged wet and dry NDVI images from long term NDVI profiles based wet and dry seasons are also very important, which contains seasonal-spectral information of different vegetation types.

Therefore, in the proposed study, MODIS satellite-based higher-temporal NDVI will be used to categorize the location-specific seasons and extract % crop area fractions or CPZs as one of the temporal images features as mapping predictor.

2.1. Spectral and Polarimetric image features for AFA mapping

S2 (a+b) satellite images are freely available with the moderate temporal and spatial resolution with multi-spectral bands, among which three red-edge (RE) bands and two SWIR bands are very useful for crop area mapping due to its sensitivity towards vegetation types and water content in the plant. Immitzer, Vuolo, & Atzberger (2016) have found that band B5, B6 (RE bands) and B11 (SWIR) bands of S2 as promising spectral channel for crop area and crop types mapping as red-edge bands show the sharp difference in between red and NIR region based on canopy pigment and nitrogen content in the plant. Rather than raw spectral channels, derived vegetation indices are prominent image features. Normalized difference indices based on narrow RE and NIR of S2 bands, as proposed by Fernández-Manso, Fernández-Manso, & Quintano (2016), have shown better adequacy for mapping burnt area and bare soil or also can be inferred as stressed vegetation area. He has proposed a simple difference band ratio of S2 narrow band B8A and B5 as NDVIre1, band ratio of B8A, and B6 as NDVIre2 and band ratio of B8A and B7 as NDVIre3, which have proved well suitability of S2 band for vegetation mapping. Similar kind of ratio index between NIR band (800 nm) and a red-edge band (710 nm) as red-edge chlorophyll index, which have a linear increase in reflectance value with an increase in plant canopy chlorophyll has been proposed by Gitelson, Gritz, & Merzlyak (2003). Later, S2 bands' suitability for calculating these indices and their prominent contribution for mapping different types of crops has been proven by Clevers & Gitelson (2013). Not only vegetation sensitive but also canopy water content-sensitive indices like Normalized Difference Water Index (NDWI) can be used efficiently to discriminate green and dry vegetation (Gao, 1996). In the usual case, natural vegetation has more stressed conditions compared to crop, which can be useful to identify via NDWI. Large scale level crop area mapping project like Sent2Agri and other studies also incorporate spectral indices like NDWI and Brightness, brightness is the square root of the sum of the square of the individual spectral band, to improve discrimination between vegetated and non-vegetated areas (Valero et al., 2016; Ouyang et al., 2017; Sevillano Marco et al., 2019).

Not only spectral aspects of S2 but also temporal aspects are important to discuss. Mohammed (2019) has used Landsat 8 data to map ACA probabilities. However, the Sentinel-2 mission provides denser time-series at a higher spatial resolution, which increases the chances of getting good quality images in growing seasons. To create an annual basis, clear dry and wet season images over the Africa region require to merge more than one type of optical datasets. For example, GSFAD30AFCE by USGS 30m cropland product over Africa merges Landsat 8 + Sentinel 2 over fixed seasons (Xiong, Thenkabail, Tilton, et al., 2017) and also Sen2Agri product by ESA uses Sentinel-2, Landsat 8 and multiple image dataset to create monthly cloud-free composites. However, it is time-consuming and not promising in the extremely high cloudy region.

On the other hand, multi-sensor based radar images (RADARSAT, Sentinel-1) combined with optical images at moderate spatial resolution also shows improvement in mapping accuracy by 3-4% due to its sensitivity to crop growth volume and cloud-free images (Blaes, Vanhalle, & Defourny, 2005; Van Tricht, Gobin, Gilliams, & Piccard, 2018). The radar backscatter measurements are not affected by clouds but are sensitive to surface roughness and moisture content, from which the structure of the feature can be depicted. The complex structured features like the forest scatter back most of the energy and appear brighter due to dense trunk, leaves, and branches. In contrast, bare soil appears darker features as it sends most of the signal away from antenna in a different direction (ESA, 2020). Talking about the moisture content in the material, materials with higher water content have higher dielectric constant and reflect a higher amount of energy appearing darker in the images (ESA, 2020). The Horizon 2020 project ECoLaSS (Evolution of Copernicus Land Services based on Sentinel data) also uses S1 and S2 images features like NDWI, NDVI, Brightness, VV/VH (radar) features for agriculture mapping and monitoring purpose. The added radar images with optical images in complex African landscapes are proven to be efficient for landcover characterization. Yet, the use of newly available S1 and S2 satellite data is less explored (Symeonakis, Higginbottom, Petroulaki, & Rabe, 2018).

2.2. Topographic image features for AFA mapping

The farming practices on the ground lead to certain distribution patterns of fields which can be explained based on terrain characteristics of the geographical area, for example, if the slope is steeper it is lower likely to have the farming practices on the ground and vice versa (Husak et al., 2008a). There are few studies have been found which used the topographic elevation and slope images to map and describe the crop distribution on the ground (Marshall et al., 2011a; Mohammed et al., 2020). Marshall et al., (2011) have found out that the elevation, which explains the position of the feature on the landscape, has explained 13% of deviance (more than slope) in expressing the arable crop area distribution across west Africa. While Mohammed et al., (2020) have found out that slope has explained more deviance than the elevation in arable field distributions.

2.3. Texture image features for AFA mapping

The human eye uses three fundamental image characteristics, textural, spectral, and contextual for identifying objects out of which, this study includes GLCM textures developed by Haralick et al., (1973). GLCM textures are easy and efficient for implementation and capture accurate texture tonal variation for central pixels, considering the surrounded pixels lie withing a window size. He proposed a total of 14 different texture features based on grey-level or single image-based spatial dependencies of pixels, out of which mainly five texture features have been used for crop mapping, those are variance, contrast, homogeneity, dissimilarity, entropy and variance (Clausi & Zhao, 2002; Gebejes et al., 2016; Haralick et al., 1973; Kim & Yeom, 2014). The variance texture feature indicates a variation in pixel intensity in the original image. The contrast texture feature indicates local variation based on the number and types of objects present in the pixel window. Homogeneity texture features indicate the higher values for bigger and continuous objects implying smooth or similar objects present in the pixel window and lower values for multiple different objects present in the pixel window. In a way, homogeneity texture features indicate the closeness of the pixel intensity values, while dissimilarity texture features indicate the opposite of it. The entropy texture feature indicates disorder in pixel intensity values meaning the homogenous area has lower entropy values. Still, on the border of the geographic object, the entropy values will be higher. These texture features help the model to improve performance by capturing finer or larger changes in the image. There are several studies have been found focusing on using texture features for mapping crop using VHS resolution images (For example, (Kim & Yeom, 2014; Neigh et al., 2018; Tokarczyk et al., 2015)) but very few studies have used texture features on moderate spatial resolution (10-20m) images. Nathaniel D. Herold, Haack, & Solomon (2004) have used RADARSAT data for mapping landcover in West Africa and found out that texture features are very important for identifying different landcover types, especially variance texture feature. Haack & Bechdol (2000) have used optical and radar images for mapping vegetation types in the East African landscape. He has found that both optical and radar image features can differentiate landcover types with similar accuracy, and for both images, texture features (especially variance texture) are very important.

2.4. Probabilistic Modelling & Mixel approach

Not only the image characteristics but also the classification techniques influence the mapping accuracy. Pixel-based supervised classification, which uses training samples (Mohammed, 2019), and unsupervised classification, which is based on error function (Enderle & Weih, 2005), assume the pixel as pure or homogeneous (Pan, Hu, Zhu, Zhang, & Wang, 2012; Smith & Fuller, 2001), meaning the only pixel represents only one type of geographic object on the surface. While mapping the crop area using this hard classification approach in fragmented and complex landscapes of Africa would have higher uncertainties due to heterogeneity within the pixel (Murmu & Biswas, 2015; Pan et al., 2012; Tran, Julian, & De Beurs, 2014). As opposed to hard classification methods, soft classification approach, or probabilistic outcomes provide better results in spectral mixture properties of pixels (Pan et al., 2012) and also explain uncertainties of classified spatial extents. The probability-based crop area maps can also be a critical input for agriculture, ecology, and water modeling applications.

As a probabilistic classification, machine learning-based algorithms like Random Forest (RF) are more efficient as, unlike the statistical model they do not assume the pre-distribution data patterns (Rogan et al., 2004) and handles the large feature datasets and noise (Debats et al., 2016a) which can improve ACA probabilities mapping. RF model is also more robust towards over-fitting compared to other machine learning algorithms due to the bagging of feature space and bootstrapping of weak learners (Breiman, 2001) and can show better predictions with easy implementation (Belgiu & Drăgu, 2016; Biau, 2012). Not only predicting the target output accurately, but also it can identify important discriminant variables in high dimensional data with efficient feature selection techniques (Gregorutti, Michel, & Saint-Pierre, 2017). RF uses the feature selection method based on the performance of the model during the learning process, which can also be referred to as an embedded feature selection method. Breiman (2001) proposed three matrices (premutation importance, Z-score & Gini Impurity Decrease) to test and evaluate the performance of the model and finally selects relevant variable from the feature samples. Out of which permutation importance is very useful in high dimension data due to existed chances of correlations between the features (Gregorutti et al., 2017). Apart from higher prediction power and feature selection technique, machines learning-based models requires a large amount of training samples which can be cost and labor intensive.

There have been very few studies found which have used RF as a probabilistic algorithm explaining the class membership probabilities for mapping vegetation cover or uncertainty in mapping. Cui, Sun, Wang, Li, & Xu (2019) have tried mapping the percentage of vegetation cover via spectral unmixing of pixel based on explained probabilities. He has compared linear and non-linear regressors for mapping percentage of vegetation cover based on cost-effectiveness and found out that RF performs as equal as other probability-based algorithms with similar error rates reported. While Loosvelt et al. (2012), have used RF classifier for landcover classification using SAR images and explained uncertainties mapped using the estimated class probabilities. He claimed that using RF algorithm based probabilities is easy to implement, and it explained lower probabilities (biased predictions) for mixed pixels. Not only for explaining uncertainties, but also RF class membership probabilities are also efficient as it helps to correct the misclassified area for mapping crop extent in complex and fragmented agriculture landscapes (Crespin-Boucaud, Lebourgeois, Lo Seen, Castets, & Bégué, 2020). Crespin-Boucaud et al., (2020) have used different spectral and topographic image features to classify irrigated crop area. He has found out that disagreements per pixel can be mapped and corrected easily via estimated multi-class RF probability and spatial-temporal rules. RF-based multi-class probabilities have also been used to map different crop types accurately, and optimized feature selection of spatial and temporal image features using RF (Yin, You, Zhang, Huang, & Dong, 2020).

2.5. Multi-source Image Features for AFA mapping

Considering the pros and cons of the different optical, radar, texture, and topographic image features, few studies have been found which asses the combined image features for mapping crop. Lebourgeois et al., (2017) have used optical simulated S2 based spectral, topographical, and texture features for mapping crop fields and have found out that high-resolution spectral image features and texture features are most prominent than the VHS (<5m) resolution based spectral, textural and topographical features. Yin, You, Zhang, Huang, & Dong (2020) have also found S2 based SWIR and RE bands are most prominent for mapping crop types. Vintrou et al., (2012) have used spectral, textural, temporal, and spatial optical features and found out that texture features are the most discriminant features for mapping crop areas in the West African complex landscape. On the other hand, (Marshall et al., 2011b; Mohammed et al., 2020) have used spectral and topographic features for mapping arable crops in the West African area and found out that spectral and topographic features are the more prominent explaining distribution of fields in the landscape. Although, none of the studies has been found out which uses all spectral, polarimetric, texture, and topographic features using open-source data for crop area mapping in complex sub-Saharan African landscape, which can be considered as a novelty of the conducted research.

3. STUDY AREA & DATA USED

3.1. Study Area

Ghana has a wide gradient of vegetation difference from north to south, which involves more forest conserved areas in the southern regions like Ashanti, Eastern, and Central. While more agriculture areas in the northern regions like Northern and Upper West. Ghana is located approximately 152 meters above sea level, bordering south shore to the Gulf of Guinea (Worldatlas, 2017). The chosen study area for the proposed research is the *Eastern region of Ghana* as it has a wide variety of topography, different types of crops and watering regimes (irrigated & non irrigated), and different land covers from north to south as shown in Figure 1. The Eastern Region is on the southeast side of the country, covering approximately 19,000 square km area. The Eastern Region was also the major producer of cassava and yam food crop in the years 2014-2016 (Ministry of Food and Agriculture (MoFA), 2017), which is also a staple food of Southern Ghana.

The region includes part of Lake Volta, which approximately divides the region in half, i.e., North (Afarm plains) and South. In the South area of the Eastern region, agro-forestry mixed landcover is dominant with the majority of cocoa, oil palm tree crops with cassava and maize arable crops. In this study, only the arable area (maize, cassava, rice) has been studied. In the Eastern region, out of total crop area, 42% area is under maize, 55% area is under cassava, and 3% area is under rice in 2016 (Ministry of Food and Agriculture (MoFA), 2017). As one can see in CPZs in Figure 1, the South area has CPZs with higher arable cropping intensity on a spatial scale comparing to Afarm plains, mainly because of wet climate or higher rainfall in southern Eastern region (Baidu, Amekudzi, Aryee, & Annor, 2017). In Afarm plains, the major landcover is agriculture and water area, where CPZs with moderate cropping intensity can be observed near Lake Volta and slightly high elevated areas implying the drier climate.

Due to the described landcover types across the region, the South area has higher rainfall intensity comparing to Afarm plains. As a result of this rainfall distribution, the South area has major rain-fed agriculture, while Afarm plains have irrigated agriculture (based on surface water). Based on the rainfall pattern, there are mainly two cropping seasons that have been followed. Those are major seasons: from March to June and minor season: from July to November. Mostly, there are no crops on arable fields during the Hamatan season across the whole region due to no rain. The Hamatan season is from November to February due to excessive heat, lack of irrigation facilities, or higher water requirement of the cops. Although, in the South area, two seasons have been followed with the intermediate dry season while in Afarm plains, due to irrigation, agriculture area near Lake Volta have the long wet season with no intermediate dry season which will be discussed further in the Results section. In this study, pixel specific MODIS temporal profiles based strata specific seasons have been included, therefore, to synthesis dry and wet seasonal images, the strata specific dry (Hamatan and intermediate short dry season), and wet seasons (major, minor) have been considered.

There is a clear difference between the Afarm plain and the south parts of the region due to high elevated mountain areas in the middle of the Eastern region, which are less suitable for agriculture. Additionally, the South area will have more hills compared to flat Afarm plains. Due to various AFA seasonality, its types, cropping patterns, and variations in elevation in the Eastern region of Ghana are well suited to understand the different behavior of satellite image features for this study.

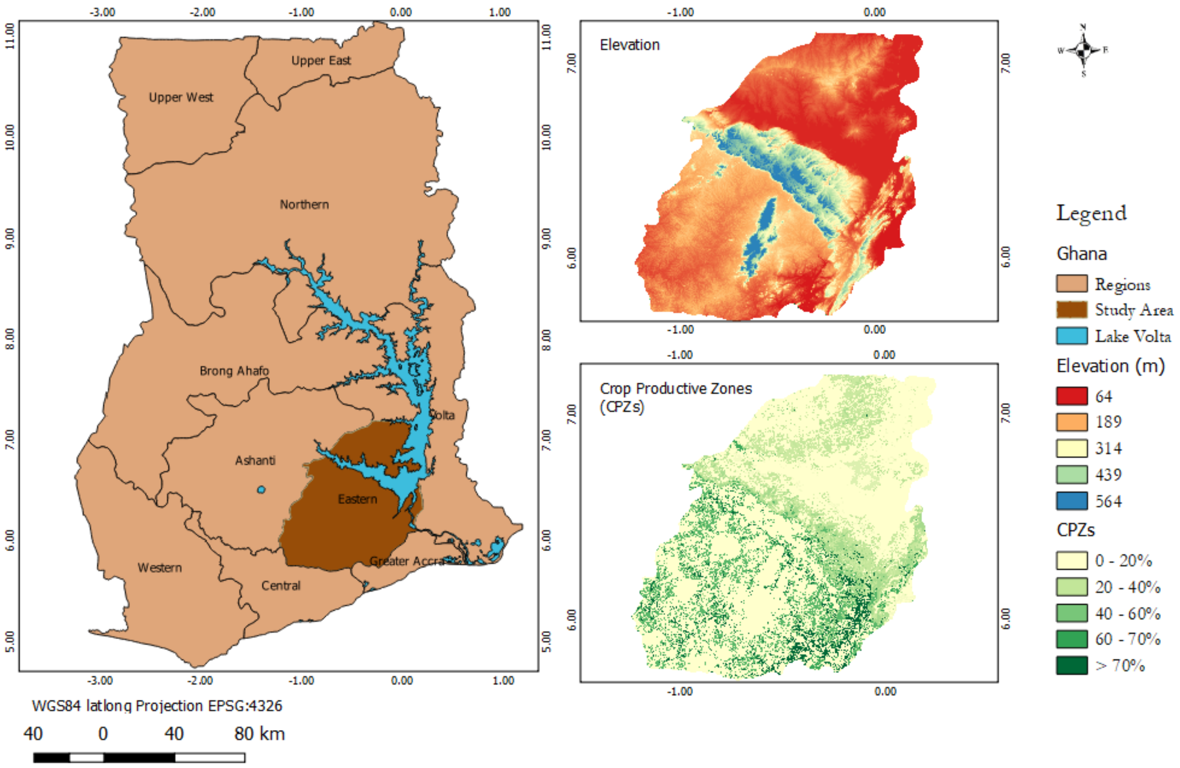

Figure 1 Study Area Map

3.2. Mapping Predictors and Reference Data

Table 1 shows a summary of the different satellite data assessed for mapping AFA. Detailed information can be found below.

Table 1 Satellite Data Used

Dataset & Source	Spatial Resolution	Temporal Resolution	Temporal Coverage (Study Specific)	Spectral Information	Properties
Sentinel-2	10m & 20m	5 days (S2a +S2b)	2017-2019	VIS (490 – 665nm), NIR (842nm) & Red-Edge bands (705 – 783nm)	More sensitive to plant chlorophyll and less sensitive to topography, soil background & atmosphere
Sentinel-1	10m	6 days (S1a +S1b)	2017 - 2019	C band IW with VV+VH polarisation	More sensitive to surface roughness and water content
SRTM	30m	-	2002	-	Sensitive to topography
MODIS	250m	16 days composite based on daily observations	2003 - 2009	VIS (459 – 670nm) & NIR (841 – 876nm)	Sensitive to vegetation (NDVI)

3.2.1. MODIS for temporal image features

MODIS Terra and MODIS Aqua composed NDVI satellite time-series images with Maximum Value Composite (MVC) of 16-day intervals, which was synthesized based on daily satellite images, from 1st January 2003 to 31st December 2009 have been used to derive seasons and CPZs which was developed by Ali et al., (2013). The spatial resolution of both Terra+Aqua images is 250m, although they sense the earth's surface on two different periods in a day with similar spectral channels (NIR, VIS, TIR) (Ali et al., 2013). He has used Vegetation Index Quality (VIQ) band to masked out haze, clouds, and other atmospheric effects to synthesize clear and denser temporal profiles per pixel. For further details, please follow the research carried out by Ali et al., (2013). In this study, MODIS Terra+Aqua pre-processed (smoothed) NDVI temporal profiles from 2003 to 2009, as developed by Ali et al., (2013) has been used to further stratification of the landscape into homogenous strata.

3.2.2. Sentinel-1 & Sentinel-2 for polarimetric, spectral and texture image features

Sentinel-1a and Sentinel-1b C band Level-1 Ground Range Detected (GRD) SAR images with dual polarisation Vertical transmit Vertical receiver (VV), and Vertical transmit Horizontal receiver (VH) (VV+VH) in Interferometric Wide swath (IW) acquisition mode has been used from the year 2017 to 2019. The temporal resolution of the S1a+S1b images is six days with a spatial resolution of 10m. For the Eastern region, only ascending images are available and included in the research. S1 (a+b) GRD images contain only information about amplitude detected, not phase information due to multi-looking processing in earth ellipsoid WGS84 projection. No additional pre-processing has been done on S1 image as Google Earth Engine (GEE) provides pre-processed S1 GRD images with GRD border noise removal, thermal noise removal, radiometric calibration, and terrain correction. The three years of images from GEE have been further used to create a dry and wet median composite of VV and VH images to create polarimetric and texture features.

In this study, Sentinel-2a and Sentinel-2b with five days interval with all bands at 20m (VIS, SWIR, RE) from the year 2017 to 2019 have been used. Due to the next launch of S2b, only S2a images are available for the study from 1st January to 1st April 2017 with ten days interval. The use of GEE for processing S2 images is limited as GEE and Copernicus; both do not provide atmospherically corrected level2A (L2A) images form the year 2017 to November 2018. Therefore, the S2 image has been manually processed using the Sen2Cor L2A processor and python. S2 L1C images for the year 2017 and 2018 have been downloaded from Earth Explorer[1], and S2 L2A images for 2019 have been downloaded from Copernicus sentinelsat API[2]. The atmospheric correction has been done on images of 2017 and 2018 via the Sen2Cor L2A processor provided by the Copernicus program. On the other hand, downloaded L2A images of 2019 are already processed by the Sen2Cor L2A processor by Copernicus. Later, the Scene Classification (SC) image at 20m is used to mask out the cloud, cloud shadow, haze, etc. to synthesis dry and wet spectral and texture image features.

3.2.3. SRTM for topographic image features

Shuttle Radar Topography Mission (SRTM) which uses two antennae based using interferometric synthetic aperture radar (InSAR) technology in a single pass to map elevation at one arc second or approximately 30m spatial resolution image of the year 2000 has been downloaded from the United States Geological Survey (USGS) to derived topographic image features. The DEM based elevation image has been further used for calculating slope in percentage.

[1] https://earthexplorer.usgs.gov/
[2] https://scihub.copernicus.eu/dhus

3.2.4. Reference data set

There are two reference data set has been used in this study, one is crop area statistics to identify higher temporal MODIS based stratified NDVI strata containing cropping intensity via CPZs, which give % of AFA probabilities at the coarser spatial resolution, and the second one is digitized crop labels for training and evaluating the performance of RF model. For stratification of the MODIS temporal profiles, the averaged cropped area from the year 2005 to 2009 of main crops in Eastern regions like cassava, maize, and rice per each district from MoFA has been used. In terms of digitized crop labels, the labels have been adopted from the DIYlandcover crowdsource platform (Estes et al., 2015) and re-modified in terms of correcting mislabelled or omitted arable fields by own visual interpretation using seasonal PlanteScope (PS) images. These labels are generated based on visual difference occurs for arable fields (crop on fields and no crops on fields) using PS images of the year 2018-2019 seasonal images in which, May to September have considered as a wet season and December to February has been considered as a dry season. Due to VHS resolution and seasonal information from PS images, the identification of arable fields was at ease. There were approximately 600 sample digitized grids with approximately 500m x 500m (same as DIYIandcover crowdsource platform) size that has been digitized with identified AFA as one and non-AFA as 0. As stratified random sampling techniques followed in this study, it is necessary to have samples in each CPZs to include to landscape-level crop intensity. Therefore, the CPZs where the digitized sample grid was not there, newly grids were generated randomly and manually digitized (see Figure 2). These sample digitized grids have been used to create pixel-level 30m sample units or polygons in the form of % of AFA present per pixel, which ranges from 0 to 1 in the form of continuous data via intersecting the sample polygon grid (30m reference grid) and digitized sample grid.

Moreover, additional validation data has been included to test the robustness of the model based on a field visit in 2020 to the southern middle Eastern region. On the ground, digitized boundaries of arable crops and non-arable crops or tree crops have been included.

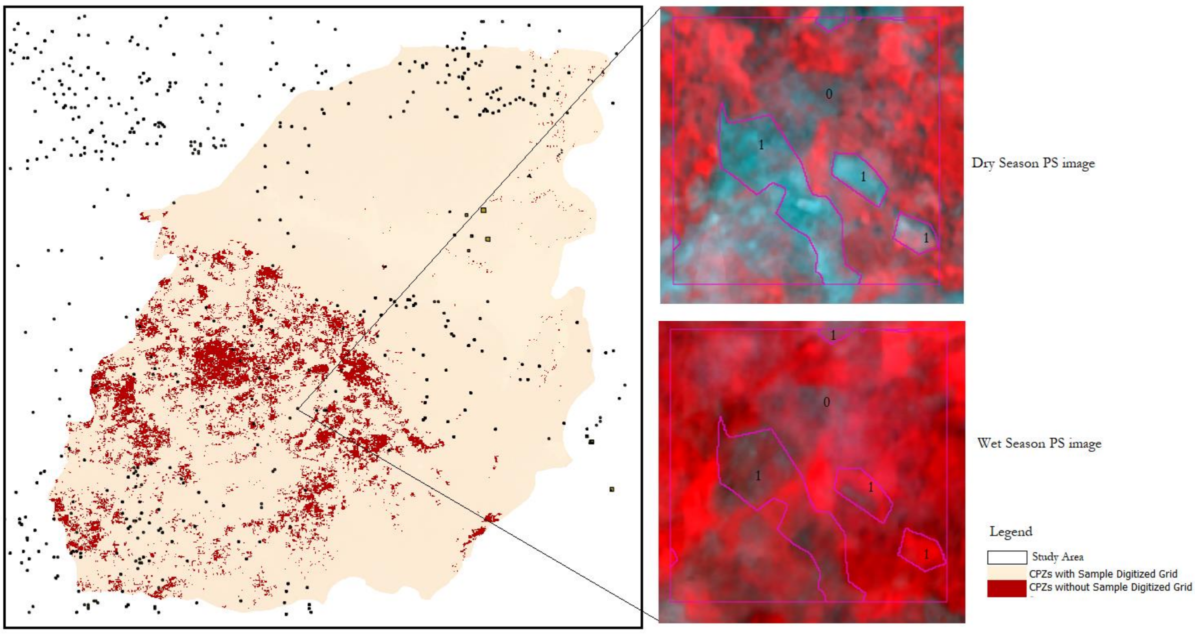

Figure 2 Sample Digitized Grids

4. METHODOLOGY

Discussing the methodology in general, as shown in Figure 3, the first step is to categorize the dry and wet seasons using MODIS long-term temporal profiles based on NDVI strata, NDVI strata is a group of pixels which have similar climatology of vegetation. Later, the strata with similar seasons have been grouped. The second step is to map cropping intensity in % of AFA via distributing the district wise crop area statistics using regression to identify strata that have an arable cropped area and to estimate AFA probabilities at 250m resolution, also called CPZs. Using the identified dry and wet seasonal period for individual NDVI strata, the long term (3 years) median dry and wet S1 and S2 images have been created. Before doing so, S1 and S2 images have been pre-processed to remove image artifacts and clouds. As an example of creating a single band dry season image, the dry season period (for example, January-March & November-December) of the individual NDVI strata is used to create a median composite image on a pixel by pixel basis from three years (2017-2019) of images. The process was followed for each stratum, and then pixel-wise masking (or merging the different strata specific dry season images into one image) on these seasonal dry median images has been carried out to create a single band-specific median image of the dry season. The same process has been followed for each band, to create dry and wet raw bands images of S1 & S2. These dry and wet raw bands images have then processed further to extract different spectral, polarimetric, texture features and snapped to 30m reference grid of DEM image at 30m resolution using different resampling techniques. SRTM based elevation image was used and processed to derive slope in % and, used as topographic features. These 30m image features' performance has been evaluated using a probabilistic RF classification algorithm to estimate probabilities of AFA per pixel further. The target map is % of probabilities of AFA, not the field boundaries as for crop yield or crop area estimation can be derived from pixel-level % probabilities with minimum cost and time required.

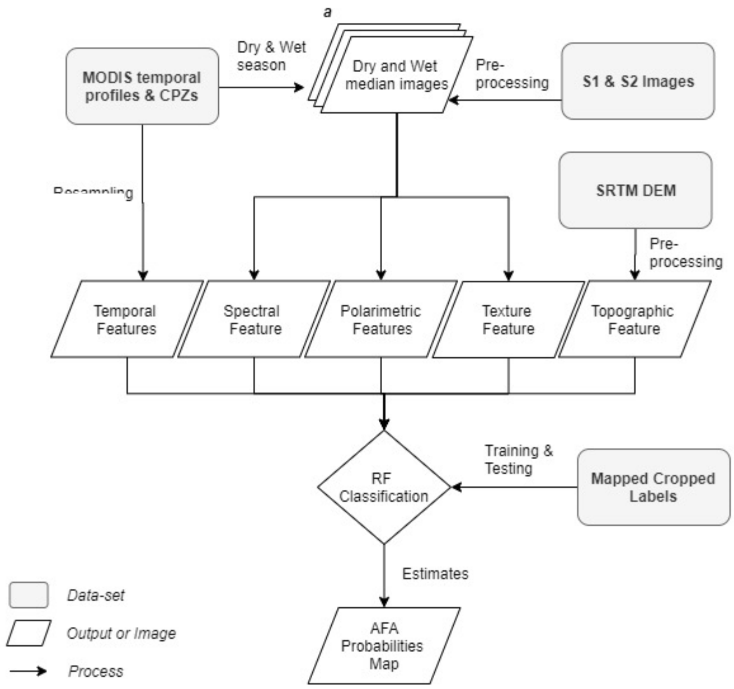

Figure 3 Generalized Flow Chart

4.1. Temporal Image Features

The higher-temporal MODIS NDVI satellite images have been used to derive two main information, one is, location-specific or strata specific dry and wet seasons, and the second one is, CPZs as % of probability of arable cropped area as a temporal image feature. To derive the dry and wet season, long-term climatology of vegetation based annual temporal profiles for the year 2003 to 2009 has been used as developed by Ali et al., (2013). Although no major or drastic land use land cover changes have happened is the main assumption for these long-term average temporal profiles based dry and wet season of the year. Ali et al., (2013) has created Maximum Value Composite (MVC) NDVI images based on temporal profiles with 16 days interval by merging Terra+Aqua images for the whole country of Ghana. He has used the Savitzky–Golay filter to smoothen these temporal profiles. To stratify the landscape into homogenous strata, ISODATA clustering has been performed, and 63 NDVI strata have been created with similar temporal profiles or seasonality throughout seven years (2003-2009). Afterward, the annual basis average temporal profiles have been calculated by averaging out the records of the same day with 16-days intervals using strata specific long-term climatological temporal profiles. These annual 63 temporal profiles later have been merged using time-series based hierarchical clustering based on Euclidean distance to identify unique seven different NDVI strata with different seasonality through the year, as an example showed in Figure 4 Merged temporal profiles of NDVI Figure 4. The complexity in processing the images has been reduced by the additional merging of these similar stratified NDVI strata. The individual strata specific NDVI profile then has been used to characterize the dry and wet season using the moving average model as suggested by Reed et al., (1994) and shown in Figure 5. The moving average of six windows (i.e., three months) has been used considering minor cropping season (from July to November) followed in the Eastern region. To calculate the moving average for the last three months of the year (October to December), the first three months (January to March) of record have been added. If the moving average intersects with the original temporal profile in an upward direction, then it is characterized as dry season until it intersects again in the downward direction. Then again, from downward to the upward direction, it is the wet season, as shown in Figure 5.

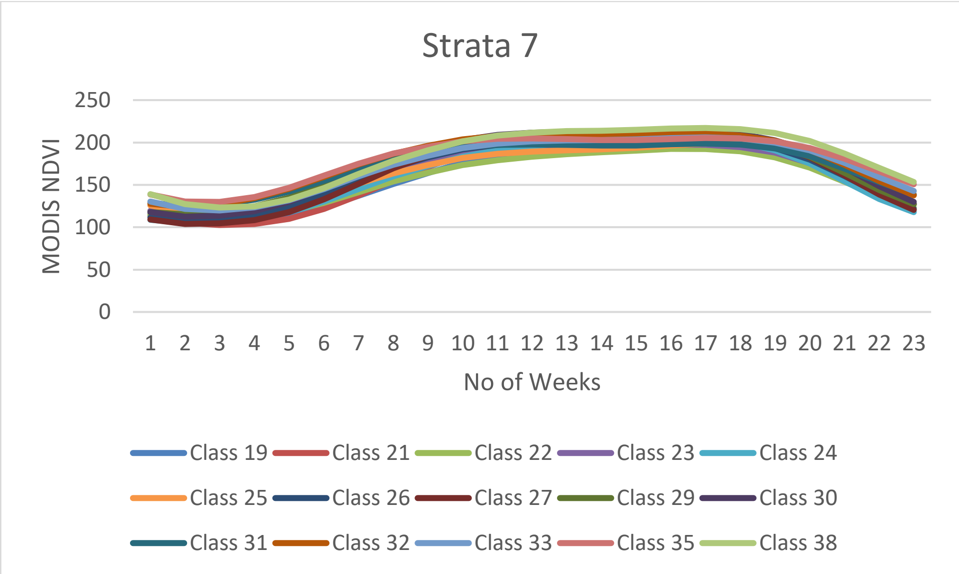

Figure 4 Merged temporal profiles of NDVI strata

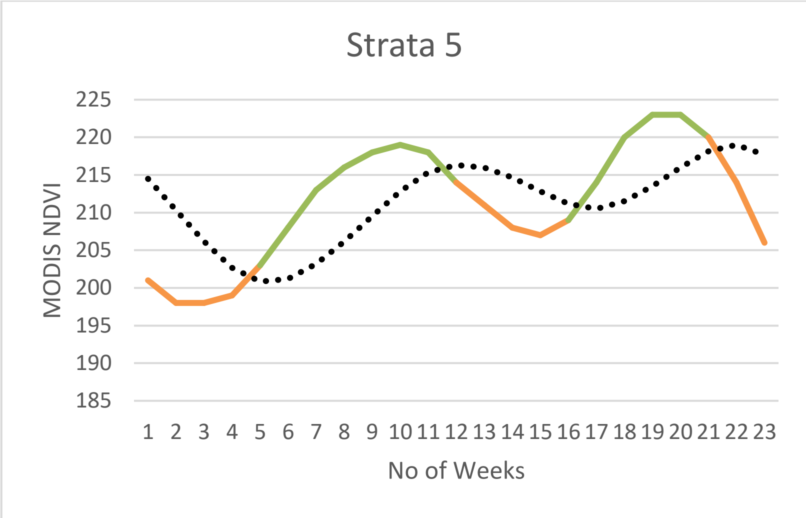

Figure 5 Moving Average for season characterization

There were total 63 strata have been created using ISODATA clustering out of which major two generalizations have been made, one is by grouping the strata which have similar temporal profiles using time series hierarchical clustering to characterize dry and wet season per each pixel, the second one is based on crop area statistics which give % of probabilities per pixel. For example, seasonal strata seven may have seasonal variation similar on a time scale with a different magnitude, which depicts the seasonal strata seven may have pixels of the arable area plus natural vegetation or sometimes forest with understory also shows variation but that strata will have zero probabilities of the crop area.

Secondly, the 63 NDVI strata have been used for the identifying CPZs or strata with % probabilities of arable cropped area in the landscape, for which, the iterative stepwise regression has been used between district wise averaged crop area statistics of the year 2005 to 2009 (as the independent variable) and calculated district-wise area of each NDVI strata falls within the district (as dependent variable) (see Figure 6). In this study, district wise area statistics of main crops like rice, maize, cassava have been included, and iterative stepwise regression has used for each crop individually and then later merged. For example, identifying strata with % probabilities of rice area, the beta coefficient has been fitted for each stratum. This fitted beta coefficient shows strata specific % probability of specific cropped area as a result of area-based stepwise regression. Since the fitted beta coefficient indicates cropped area probabilities, the negative beta coefficient is not relevant; therefore, it is necessary to remove those strata and re-run the stepwise regression. The same process has been followed for each iteration of regression until all the beta coefficients are non-negative. This whole process has been followed again for rice, maize, and cassava and identified the final % of probabilities of each cropped area in each stratum. Later, only significant beta coefficient with p-values < 0.05 are included. Since this study does not focus on mapping crop types, the significant % of cropped area per strata (rice, maize, cassava) have been merged as % of the arable cropped area as CPZs. It is important to note that stepwise regression has been used on country level area statistics and later clipped only to study area to increase the confidence in the mapped beta coefficient. The strata which are not identified as significant (Confidence Inteval:95%) % of the arable cropped area are included as 0% of probabilities of the cropped area. These MODIS based 250m CPZs have been snapped to 30m reference grid of DEM images at 30m using the nearest neighborhood resampling technique.

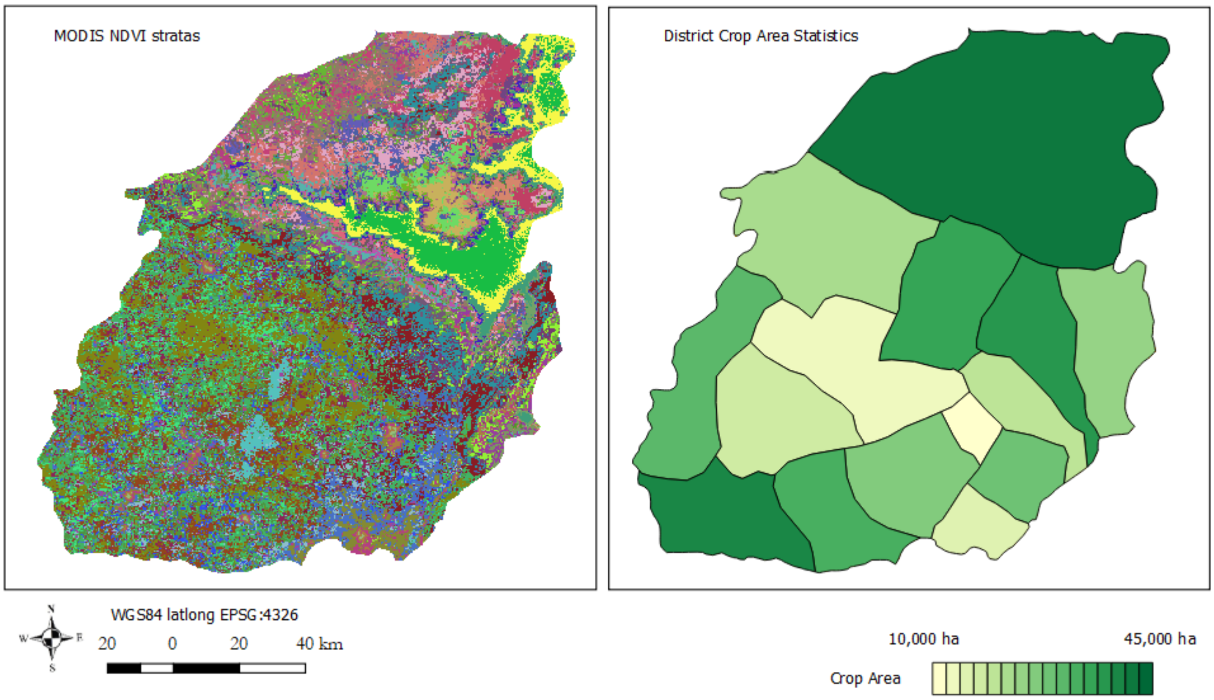

Figure 6 NDVI strata & Crop Area

4.2. Spectral Image Features

Top of the Atmosphere (TOA) S2 (a+b) images of the years 2017 and 2018 have been downloaded and atmospherically corrected using the Sen2Cor L2A processor to create Bottom of the Atmosphere (BOA) images using command line operator. Downloaded images of 2019 images have already been atmospherically corrected. The atmospheric correction results in VIS & NIR bands at 10m, excluding RE and all bands at 20m, including RE. In this study, 20m, all bands images have been masked out to remove the cloud, cloud shadow, and haze using 20m Scene Classification (SC) images, which are classified map of the individual scene by L2A processor.

Each NDVI strata (total seven seasonal grouped strata) specific dry and wet season images of each band have been created by taking the median of all the 2017, 2018, and 2019 images using Python. In the end, a total of 9 bands of the dry season and nine bands of wet season images have been created. These 18 images have later been snapped to 30m reference grid of DEM images by bilinear resampling method, which averages out nearest four pixels. The original images of S2 images are in UTM projection, which has been re-projected to Ghana Metre Grid local projection (EPSG:25000).

As discussed in 2.1, raw bands of dry and wet season images have used to create spectral image features by ratio different band combinations, as shown in Table 2, which are widely used in crop area mapping. Therefore, there is a total of 14 spectral features have been used in the model to evaluate its performance.

Table 2 Spectral Feature Equation

Spectral Feature	Equation	Reference
Normalized Difference Vegetation Index	$\mathrm{NDVI} = \frac{\mathrm{NIR\ B8} - \mathrm{Red\ B4}}{\mathrm{NIR\ B8} + \mathrm{Red\ B4}}$	(Tucker, 1979)
Normalized Difference Vegetation Index red-edge 1 narrow	$NDRE1 = \frac{\mathrm{NIR\ B8A} - \mathrm{Red\ Edge\ B5}}{\mathrm{NIR\ B8A} + \mathrm{Red\ Edge\ B5}}$	(Fernández-Manso et al., 2016)
Normalized Difference Vegetation Index red-edge 2 narrow	$NDRE2 = \frac{\mathrm{NIR\ B8A} - \mathrm{Red\ Edge\ B6}}{\mathrm{NIR\ B8A} + \mathrm{Red\ Edge\ B6}}$	(Fernández-Manso et al., 2016)
Normalized Difference Vegetation Index red-edge 3 narrow	$\mathrm{NDRE3} = \frac{\mathrm{NIR\ B8A} - \mathrm{Red\ Edge\ B7}}{\mathrm{NIR\ B8A} + \mathrm{Red\ Edge\ B7}}$	(Fernández-Manso et al., 2016)
Chlorophyll Index red edge	$\mathrm{CLre} = \frac{\mathrm{Red\ Edge\ B7}}{\mathrm{Red\ Edge\ B5}} - 1$	(Gitelson et al., 2003)
Normalized Difference Water Index	$\mathrm{NDWI} = \frac{\mathrm{NIR\ B8A} - \mathrm{SWIR\ B12}}{\mathrm{NIR\ B8A} + \mathrm{SWIR\ B12}}$	(Gao, 1996)
Brightness	$\mathrm{Brightness} = \mathrm{sqrt\ of}\ (\frac{\mathrm{Red\ x\ Red}}{\mathrm{Green\ x\ Green}})/2$	(Escadafal, Girard, & Courault, 1989)

4.3. Polarimetric Image Features

Pre-processing and creating seasonal S1 images have been done using Google Erath Engine (GEE). Since S1 GRD VV and VH ascending images are available at 10m resolution by GEE and have already been processed by radiometric and terrain correction, no additional further pre-processing has been done. NDVI strata-specific dry and wet zone seasonal VV and VH images have been created with similar process steps followed for S2 images. The speckle filtering of S1 images has not been included as a pre-processing step. Still, it can be considered in the way of snapping dry and wet VV, VH bands to 30m reference DEM grid by cubic convolution resampling techniques which average out nearest 16 pixels.

As shown in Figure 7(b), the S1 radar image shows very bright pixels on the edges of the high terrain area due to the viewing geometry of the satellite images Figure 7(a). Therefore using the SRTM based DEM image, slope, and aspect has been calculated. The mask of the potential foreshortened pixel at 30m resolution has been created, as shown in Figure 7(c). The mask has been created using GEE as developed by Kakooei, Nascetti, & Ban, (2018). These masked VV and VH images, including difference (VV-VH), addition (VV+VH), and the ratio (VV/VH) of these two bands, have included a total of 10 polarimetric image feature.

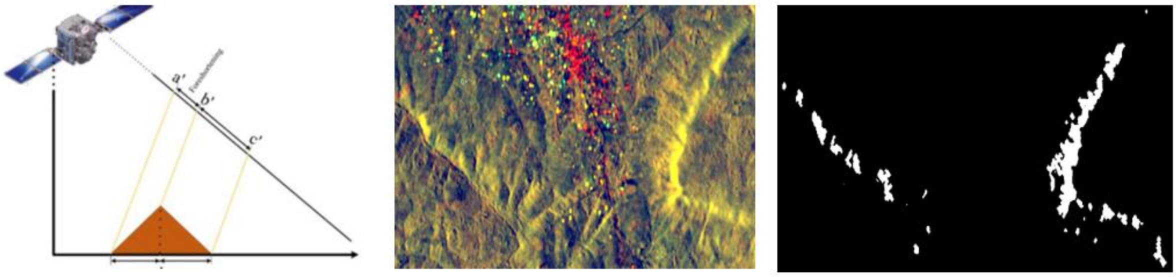

(a) Foreshortening

(b) S1 Dry season image (RGB: VV, VH, VV/VH)

(c) Foreshortening Mask at 30m

Figure 7 Radar Foreshortening & Mask at 30m, (a) is adopted from (Kakooei et al., 2018)

4.4. Textural Image Features

The GLCM techniques based optical and radar image features have been calculated on raw 9 bands of S2 images and VV, VH images of S1 images at 30m resolution for the dry and wet season. Zakeri, Yamazaki, & Liu (2017) have tried several window sizes from 3x3 to 21x21 in the complex landscape for landcover mapping using S1 images and showed that there we minimal changes in improvement in accuracy after the 11x11 window size. Therefore, the window size of 11 has been considered to include neighborhood pixel intensity for the heterogeneous landscape. Also, in terms of considering pixel intensity in all angles of the surrounded pixels concerning central pixel, average values in all angles with one angular displacement value have been calculated considering the fragmented geographic landscape. Rather than raw averaged quantizer, a probabilistic quantizer based on actual occurrences of pixel intensity values has been used and provided by SNAP. To calculate texture features, only raw bands of S1 (VV, VH) and S2 (VIS, RE, SWIR) images have been considered, the modified spectral or polarimetric based features may give the similar texture intensity value, therefore, not included to avoid extra computational efforts.

There are usually five main GLCM textures that have been considered for AFA mapping those are, Homogeneity, Dissimilarity, Contrast, GLCMvariance, and Entropy (Haralick et al., 1973; Kim & Yeom, 2014). Therefore, in this study as well, a total of five GLCM texture per each band and seasons have been calculated. In total, there 110 texture features have been included in the study. There is no need for additional snapping as the raw snapped bands of S1 & S2 at 30m have been used.

4.5. Topographical Image Features

SRTM based DEM images at 30m have been downloaded, from which slope in % have been calculated. The slope in percentage has been calculated using ee.Terrain package provided by GEE, which used elevation and aspect. Further details can be found here[3]. Since the target resolution of the AFA map is 30m, the DEM image been used as a reference grid in the study, other images like S1 and S2 images have been snapped to the DEM grid. The elevation (m) and slope image were used as a topographic image feature.

4.6. Mapped Cropped Labels

As discussed earlier, approximately 600 sample digitized grids with AFA (value 1), and non-AFA (value 0) labels have been used to derive 30m pixel-level samples showing % of AFA. The 30m samples showing % AFA (continuous data) have been derived by intersecting the sample digitized grids with a 30m sample polygon grid (reference 30m DEM grid). To derive, pixel-level % AFA samples, as a first step, non-overlapped or partially overlapped 30m grid cells (from sample polygon grid) on individual sample digitized grid have been discarded. These grid cells are mostly at the boundary of the sample polygon grid and do not always include underneath the digitized sample grid fully. Afterward, the 30m sample polygon grid has been intersected with the digitized sample grid to calculate the % AFA area, as shown in Figure 8. There are approximately 93,230 pixels or samples that have been used in the model. The majority of the pixels are either 0% or 100% probability of AFA. In the end, there was a total of 59,980 samples for training and 25,631 samples for testing.

Additional validation dataset or ground truth boundaries have been collected, and a similar process has been followed. A total of 67 sample points have been used as independent validation data for assessing the robustness of the RF model.

[3] https://developers.google.com/earth-engine/tutorial_api_03

0	0	0	0	0	0	0	0	0	0	0	0	0	0	0	0	0	0
0	0	0	0	0	0	0	0	0	0	0	0	0	0	0	0	0	0
0	0	0	0	0	0	0	0	0	0	0	0	0	0	0	0	0	0
0	0	0	0	0	0	0	0	0	0	0	0	0	0	0	0	0	0
0	0	0	0	0	0	0	0	0	0	0	0	0	0	0	0	0	0
0	0	0	0	4	25	40	20	1	0	0	0	0	0	0	0	0	0
0	0	26	22	9	99	100	100	68	0	0	0	0	0	0	0	0	0
0	3	42	22	0	82	100	100	33	0	0	0	0	0	0	0	0	0
0	0	0	0	13	84	87	91	2	0	0	0	0	0	0	0	0	0
0	0	0	15	54	23	4	25	22	50	1	0	0	0	0	0	4	29
0	0	0	0	0	0	0	3	92	100	63	0	0	0	0	1	73	76
0	0	0	1	0	1	3	0	34	36	7	0	0	0	0	0	34	77
41	0	0	46	61	69	46	0	0	0	0	0	0	0	0	0	0	5
86	34	0	0	0	9	6	0	0	0	0	0	10	54	3	0	0	0
27	24	0	0	0	0	0	0	0	0	0	0	86	100	48	0	0	0
0	34	6	0	0	0	0	0	0	0	0	0	80	100	89	2	0	0
19	100	45	0	0	0	0	0	0	0	1	45	90	93	19	0	0	0
12	87	20	0	0	0	0	0	0	0	49	57	16	19	0	0	0	0

Figure 8 30m Sample Grid

4.7. Probabilistic Random Forest Model

Ensemble RF algorithm has gained more popularity in ML as it is less prone to over-fitting with lower bias & variance due to multiple decision trees and random sub-sampling of features and observations (also called bagging) (Belgiu & Drăgu, 2016). Because of multiple decision trees, the lower bias on the training sample and lower variance on testing samples can be achieved, which increases the accurate predictions. In this study, the RF algorithm has been used not only because of its higher prediction power, but also it is easy to implement, understand, and has capabilities to identify relevant feature space in high dimensional feature space.

As discussed in section 2.4, few studies have used RF regressors to estimate the percentage cover of vegetation per pixel. In contrast, other studies have used RF classifier based probabilities via spectral unmixing for mapping vegetation per pixel. In this study, as discussed in 4.6, the majority of the pixel at 30m resolution follows under the 0% actual probabilities or 100% actual probabilities of AFA and very minimal (only 10% pixels out of all pixels) sample does not have pure actual probabilities per pixels. While predicting % probabilities per pixel using RF regressor based on the mean of all tree-based predictions can be misleading where sample data falls near binomial distribution. On the other hand, % probabilities of per pixel (p(i)) using RF classifier, have been defined by the following equation,

$$p(i) = \frac{k(i)}{k} \qquad (1)$$

Where k(i) is the total no of trees with positive prediction, i.e., class 1 or AFA, and k is the total no of trees used in the model. Since the sample data follow the approximate binomial distribution of the probabilities, the model can be more accurate for predicting 0 and 1 and assuming that, remaining uncertainty or mixed the pixels can be better explained via mapped probabilities based on class membership probabilities rather than considering every number of trees predictions in regression trees. That is why, in this study, the RF classifier has been used to map % probabilities of AFA, which uses binomial distribution as a tree split criterion.

In this study, RF classification has been used as a binomial classifier to map the probability of AFA per pixel. As discussed in 4.6, the only samples with 0 (non-AFA) and 1 (AFA) have been considered. These sample data have further split into a 70%-30% ratio as training and testing data. Due to the high dimensionality of the feature space with a total of 137 image features, it was necessary to select relevant and valuable features and train the final model with only important features. RF model provides three matrices to evaluate variable importance. Those are permutation importance, Z-score, and Gini Impurity Decrease (Breiman, 2001). Among which permutation importance and Gini Impurity Decrease are popular for relevant feature selection. Permutation importance shows the direct link between independent feature and the target feature via explaining the decrease in error rate due to individual features for prediction of the target response. The decrease in error rate can be calculated via predicting out-of-bag samples (OOB) (samples which are not used for training the specific tree), by removing the variable from OOB feature space.

On the other hand, Gini Impurity Decrease is based on the quality of the splitting of the feature space for training the model (Hastie, Trevor, Tibshirani, Robert, Friedman, 2009a). For the feature space with high dimensions have higher chances of correlated features for which permutation importance matrix can be relevant as it directly shows the change in the target response variable (Gregorutti et al., 2017). Therefore, to select relevant image features, premutation importance has been implemented as a recursive feature elimination (RFE) technique with a surrogate or dummy RF model trained with 5 fold cross-validation and 500 number of trees.

Since the target output is predicted probabilities of AFA rather than classified labels per pixel, the feature selection surrogate RF model has used loss function based on probabilistic Brier Score (BS), BS score explains uncurtaining, and reliability based on the difference between actual and predicted probabilities. Predictions. BS can be interpreted as the means squared error (MSE) between actual and predicted probabilities (Brier, 1950; Brownlee, 2018). Therefore, in this study, the relevant features have been selected based on the model trained with a mean decrease in BS per each fold.

Based on the outcome of the feature selection process, relevant features are then used for training the final model. The final RF model has been trained with two hyper-parameters (parameters which can change the model performance), those are, total 500 number of trees, and the maximum feature to select for random sub-sampling is the square root of total feature, as suggested by Belgiu & Drăgu (2016). Since as discussed in 4.6, the sample data frame is highly imbalanced, meaning it has 10 times more samples of non-AFA compared to AFA samples. That is why the model has been trained using cost-sensitive learning (higher weight to wrong predictions of AFA area) base on class weights given to non-AFA and AFA as 0 and 3, as suggested by Chen & Liaw (2004). The weights are derived based on class frequency in total sample data.

The model performance has been evaluated on a 30% testing dataset and additional validation data set, which is based on ground measurement in the year 2020. The mapped probabilities have been normalized to 0 and 1. The mapped probabilities map has been masked with the Global Human Settlement (GHS) layer of 2015 at 30m to mask out urban and water areas. The model has been evaluated on dummy class labels using Area Under Curve (AUC) Receiver Operating Characteristics (ROC), error matrix with precision, and recall. The mapped probabilities have been evaluated based on BS and pseudo R^2. The pseudo R^2 has been calculated based on percentage variance explained in observed and predicted probabilities, as mentioned in Coulston et al., (2012). Partial Dependence Plots (PDP) have also been plotted to understand the relationship between image features and mapped AFA probabilities (Hastie, Trevor, Tibshirani, Robert, Friedman, 2009b). PDP explains the partial behavior of the dependent variable (here image feature) with the change in independent feature (AFA probabilities) over a selected range.

5. RESULTS

5.1. Temporal Image Features

As discussed in Methodology, the higher temporal MODIS based long-term averaged annual NDVI temporal profiles have been used to identify a total of seven different NDVI strata or agro-ecological zones which have to distinguish seasonal changes identified using time-series based hierarchical clustering of total 63 NDVI strata. Although in general, the starting of the wet or sowing season usually starts in March and ends in either June or November, as shown in Figure 9. In some areas there were two dry seasons in the year have been observed which is in starting and ending of the year, however in few regions there will be intermediate dry seasons (July or August) can be observed (strata 5 & 6), especially where irrigation facilities are obscured due to subsistence farming and seasonal rivers.

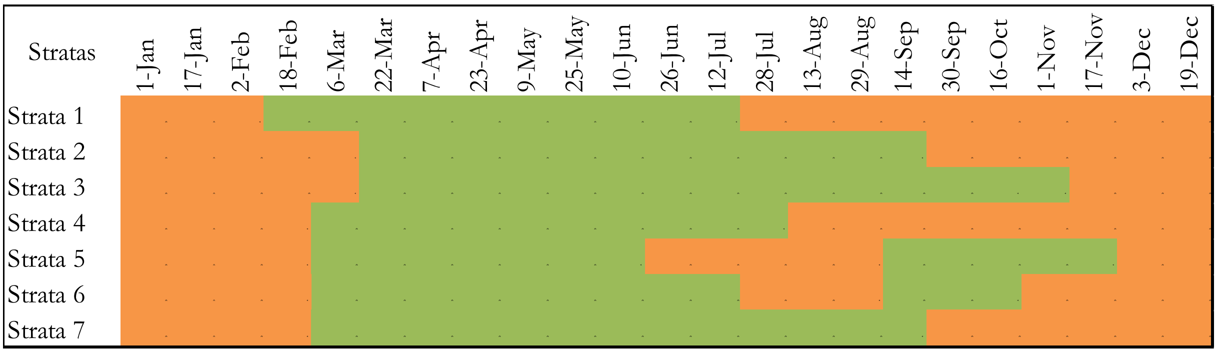

Figure 9 Strata's Seasons

Continuing with the NDVI strata, the NDVI annual temporal profiles explaining dry and wet season also reflects an on-ground arable farming system in a specific agro-ecological zone. For example, as shown in Figure 10, the area near Lake Volta, i.e., strata 7, usually have a long wet season from March to November due to the availability of surface water for irrigation. The irrigated arable area in the north or near lake follow the start and end of the season same as non-irrigated area in the south, however, in the south (strata 6) usually, two seasons have been followed, that is major (March to June). Minor season (August to November) with the intermediate dry season (June-July) as the majority of the area is rain-fed agriculture. Based on Figure 9 & Figure 10, the different dry and wet seasons have been followed across all-region. Getting a seasonal variation is very important to the map AFA area that is why agroecological zone-specific seasons have been used to create dry and wet season texture, spectral and polarimetric image features.

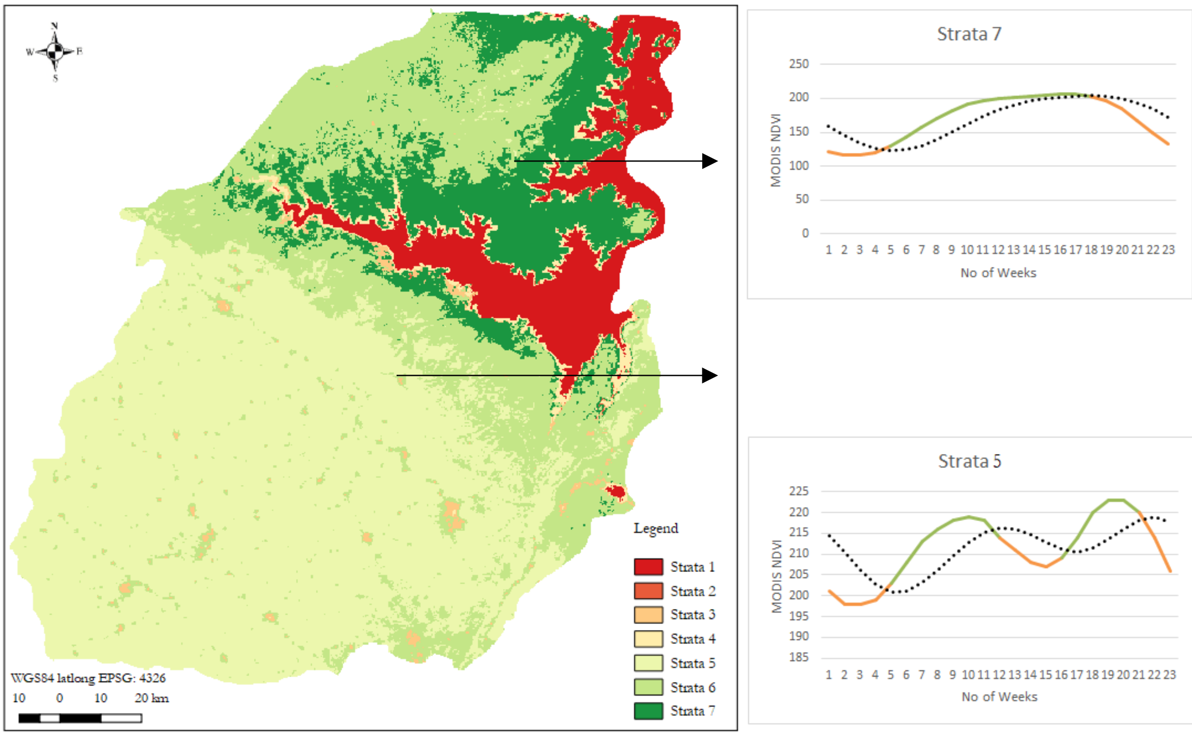

Figure 10 Seasons & NDVI strata

Higher temporal based NDVI strata were also used to derive probabilities of AFA at 250m from MODIS images combined with district wise AFA area statistics using stepwise regression as discussed in Methodology. There were a total of 19 NDVI strata have been found significant (p values=<0.05) combined with rice, maize, and cassava crop probabilities. There are few strata (52 & 59), which have significantly explained probabilities for all crops. In the research, summed up probabilities of rice, maize and cassava have been considered, which gives a total of 15 unique CPZs or merged NDVI strata derived from 19 NDVI starts. For example, NDVI starts with similar AFA probabilities like strata 9, and 10 are merged and considered as one CPZs with 5% probabilities of AFA.

Table 3 CPZs (NDVI strata + significance)

NDVI Strata	Rice Probabilities	Maize Probabilities	Cassava Probabilities	Total AFA probabilities (%)	Significance (p-value =< 0.05)
3	3	-	-	3	0.03
4	9.3	-	-	9	0.00
8	-	11.2	-	11	0.01
9	-	5.3	-	5	0.04
10	4.5	-	-	5	0.00
14	-	-	8.1	8	0.01
25	3	-	-	3	0.00
27	-	10.2	-	10	0.00
33	-	-	20.4	20	0.00
35	-	-	15.1	15	0.00
37	3.4	-	-	3	0.04
44	-	-	51.1	51	0.00
45	-	16.6	-	17	0.00
46	-	22.7	-	23	0.01
50	-	-	16.6	17	0.00
51	-	13.8	-	14	0.05
52	-	34.1	37.3	71	0.00 (Maize), 0.00 (Cassava)
54	-	23.5	-	24	0.00
59	5.1	14.4	23.5	43	0.00 (Rice, Maize), 0.00 (Cassava)

As shown in Figure 11, a different 15 CPZs have been identified. The higher intensity of arable crops observed in southeast and areas near Lake Volta and lower intensity of arable crops observed in the northern area. The main reason is a rainfall distribution over the region where Afarm plains have lower rainfall intensity indicating a dry hotter climatic region. In comparison, the southern area has higher rainfall intensity.

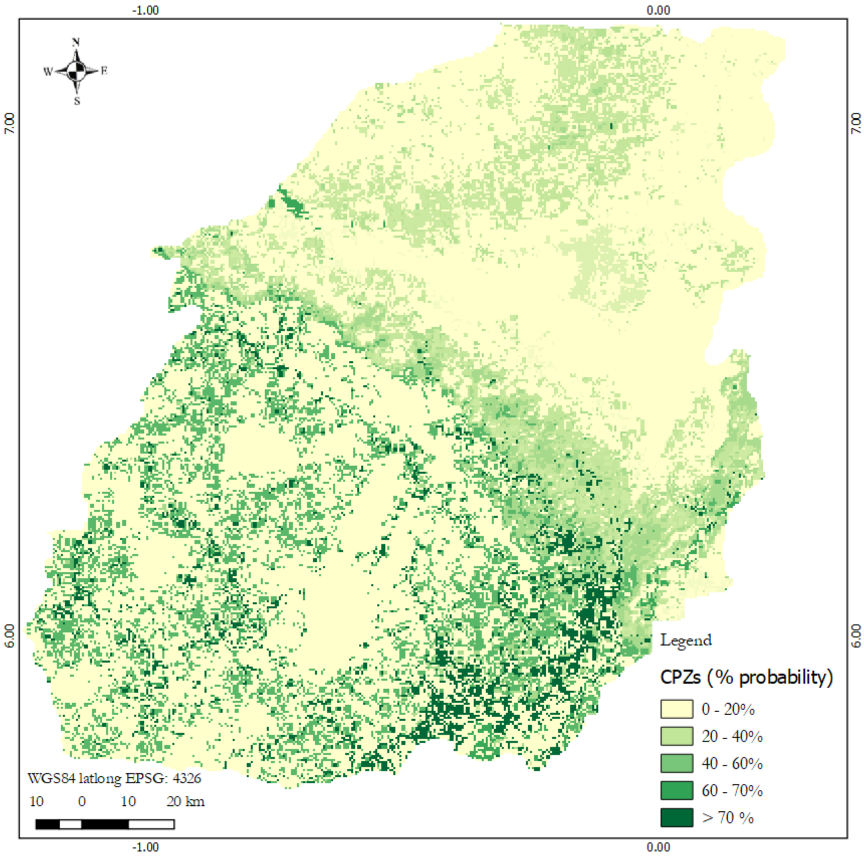

Figure 11 Crop Productive Zones (CPZs)

5.2. Spectral, Texture and Topographic Image Feature

One of the major problems with optical sensor image is cloud cover, which has been addressed by taking a median of the 2017 to 2019 S2 images. The median of the images has been taken over the NDVI strata specific seasons to create wet and dry season images, as shown in Figure 12, resulting in cloud-free images in West Africa with clear pixels change for AFA in the dry and wet season. As an example, a part of the Easter area has been zoomed in the image, and the area lies within NDVI strata 5.

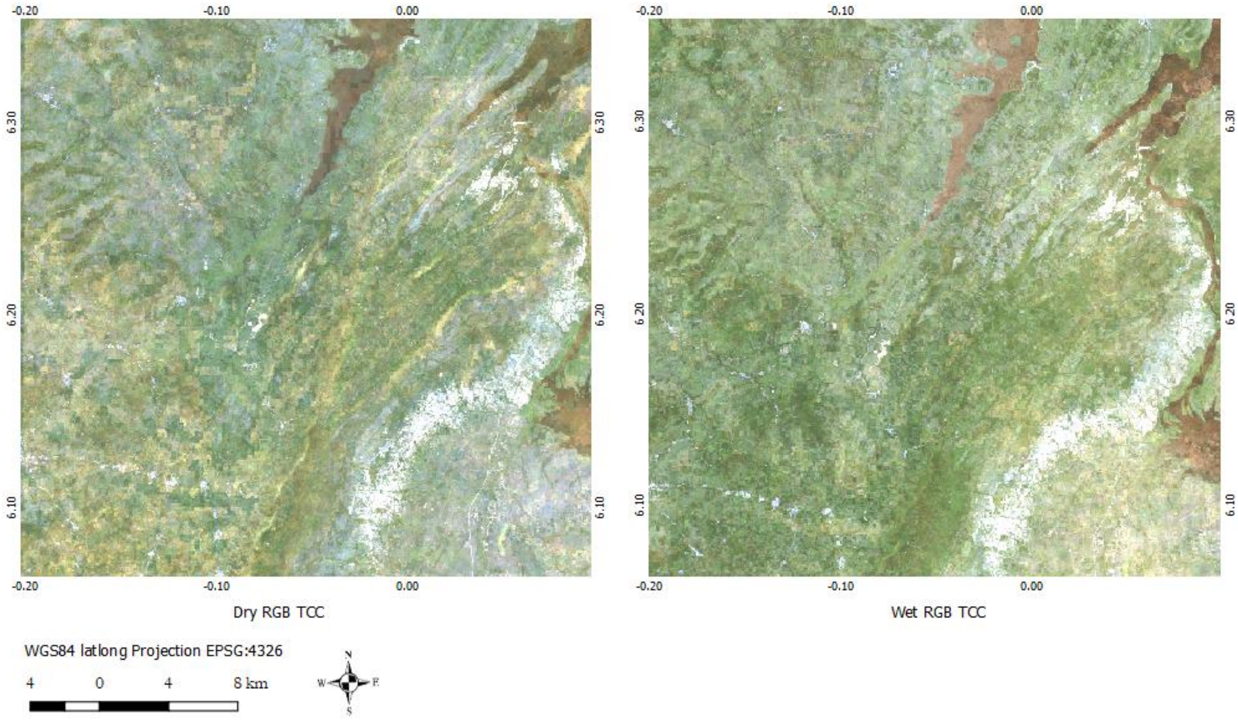

Figure 12 S2 cloud-free Dry and Wet Season True Colour Composite (TCC)

Apart from temporal, S2 based spectral and S1 based polarimetric features, S1 and S2 raw bands based five texture features have been used. Each texture feature has distinguished characteristics, as shown in Figure 13, where the PS False Colour Composite (FCC) image (for clear visualization purpose) with five different texture features have included in part of the Eastern area. In the image, forest area or tree crops have lower variance, contrast, dissimilarity, and entropy due to smooth or compact homogenous pattern resulting lower variation are considered a group of pixel window, while for cropped and urban areas are it is opposite due to heterogeneity in agriculture landscape. Out of these texture features, variance texture features showed clear edges and differences between different types of vegetated areas.

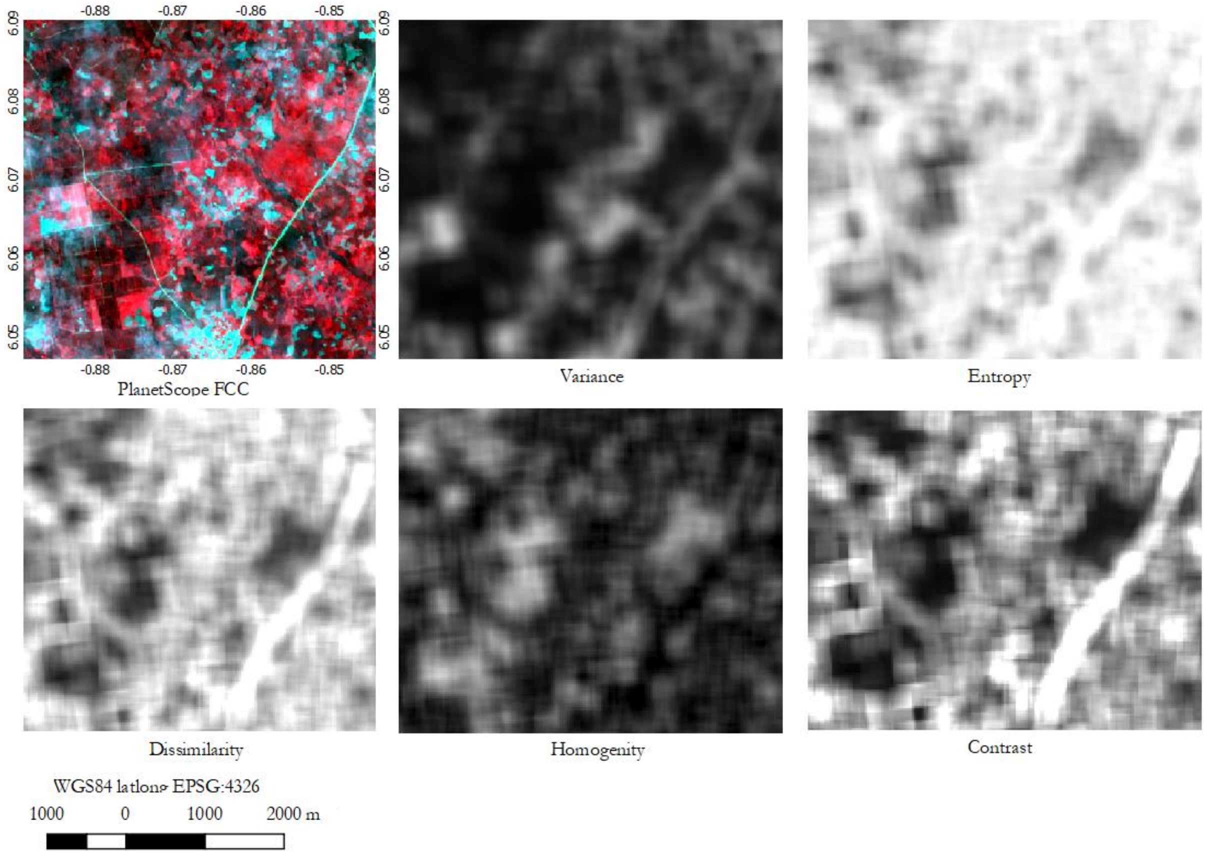

Figure 13 Texture Features (SWIR band)

Topographic elevation and slope features also showed unique insights into the landscape; for example, the southern areas have lots of hills compared to the northern area, which can be observed in Figure 14. Although, the steepness of these hills is marginal (0-10%) except only in the high elevated area (approximately >550m), which has steepness more than 35%. In general, no crops can be conserved on higher elevated areas, whereas in lower elevated or hilly areas in southern areas generally have cassava and maize crops. In contrast, in the northern or flat areas have maize, rice, or vegetable crops.

.

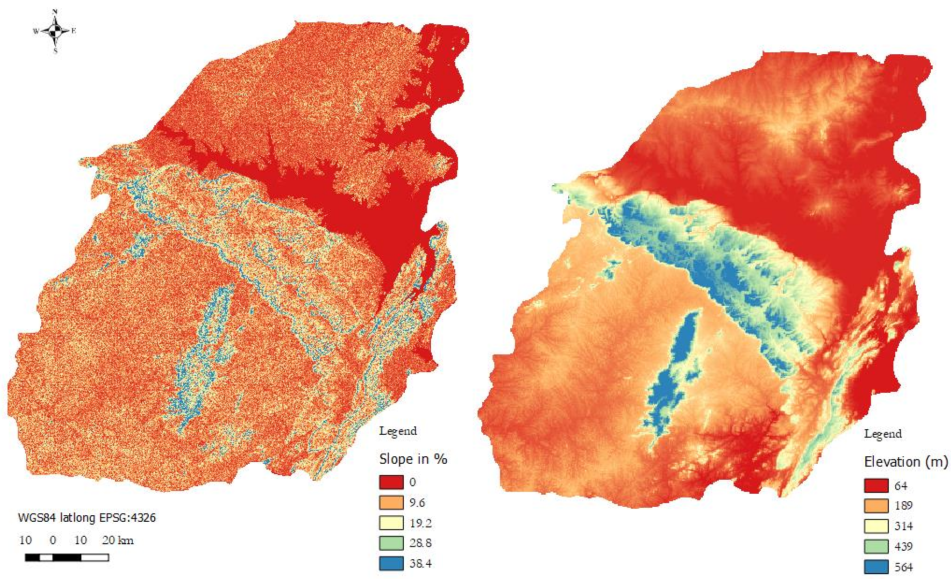

Figure 14 Topographic Image Features

5.3. Important Mapping Predictors

As discussed in Methodology, the AFA at 30m target resolution has been estimated using RF. RF algorithm is a very handful in terms of feature engineering or selecting the relevant variables as unlike the traditional filter-based methods (commonly used one is Pearson correlation coefficient) the decision trees select the relevant features based on learning algorithm performance by splitting the feature space randomly by rows and columns (Gregorutti et al., 2017). In this study, there are a total of 137 (1 temporal, 2 topographic, 14 spectral, 10 polarimetric, and 110 texture) image features that have been included.

Therefore, as suggested by Gregorutti (2017), RFE technique with 5 fold cross-validation has been used as a wrapper method to identified stable and discriminant relevant features in high dimensional and correlated feature space. The BS (as explained in Methodology) has been used as a scoring metric to train and test each fold. Permutation importance or Mean Decrease in Error (MDE), showing a mean decrease in probabilistic BS score by individual variable, has been considered to select relevant features. As shown in Figure 15, there are total 36 variable has been selected for estimation of AFA, after the 36 features, the marginal increase in BS error can be observed, implying that the rest of the features are not relevant discriminants or act as noise features for estimating probabilities of AFA and are further leading to overfitting of the model.

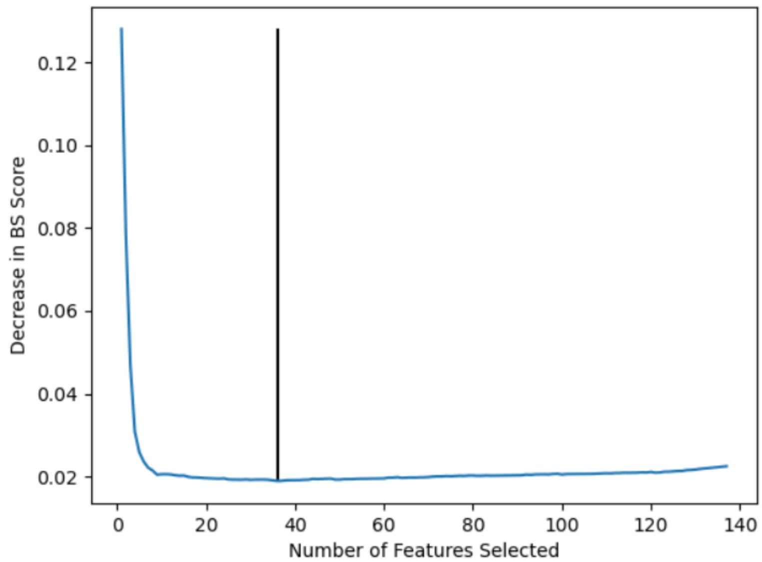

Figure 15 Mean Decrease in BS Error and Feature Selection

Total 36 important features have been selected out of which 33 features are texture features (majorly Variance texture), 1 is topographic (Elevation), 1 is temporal (CPZs), and 1 is polarimetric (Dry VV) image feature. These features, in general, can be grouped (see Table 4) where topographic and texture features, in general, improve prediction by reducing 0.14 to 0.10%, temporal CPZs feature reduces 0.05%, and polarimetric feature reduces 0.04% in BS score. The values of BS scores range from 0 to 1; therefore, the percentage decrease (reduced BS score * 100) reduces in error and has values between 0% to 1%.

Table 4 Important Image Feature

Group No	Feature Names	% decrease in (BS score)	Type of Feature
1	Elevation & Wet SWIR (B11) Variance Texture	0.11 – 0.14%	Topographic & Texture
2	Wet B12 & Dry B12, B11, B07, B06 Variance Texture	0.06 – 0.10%	Texture
3	Wet VV & Dry VV,B8A Variance Texture, CPZs	0.05%	Texture & Temporal
4	Dry B02, B05 & Wet B04, B05 Variance Texture, Wet B07 & Dry B06 Entropy Texture, B06 Homogeneity Texture, Dry VV	0.04%	Texture & Polarimetric

As shown in Figure 16, elevation has been found the most important variable, 0.14% MDE. One of the main reasons could be the terrain characteristic of area and farming practices followed on hilly areas in the Eastern region. Considering MDE, following to elevation, the next important 9 image features are variance texture features, among which wet SWIR bands (B11, B12), dry narrow RE & NIR bands (B6, B7, B8A), dry and wet VV bands are most important as it has improved model performance by approximately 0.06% to 0.10% decreased error in BS score. Out of total 36 features, majority dry season based image features, which are in total 18, plays an important role followed by wet season based image features, which are in total 16. As observed in Figure 16, there is minimal difference in MDE and shows almost equal importance for a group of features, for example, dry, and wet VV variance, dry B8A variance, and wet B06 homogeneity and CPZs have similar MDE score with very few decimal changes and are approximately equally important for estimating AFA. The same conclusion can be made for another group of features as well from the graph or above table.

In general, the topographic elevation and optical and radar-based texture feature outperformed the spectral features. It also outperformed a temporal and polarimetric image features in a way as well.

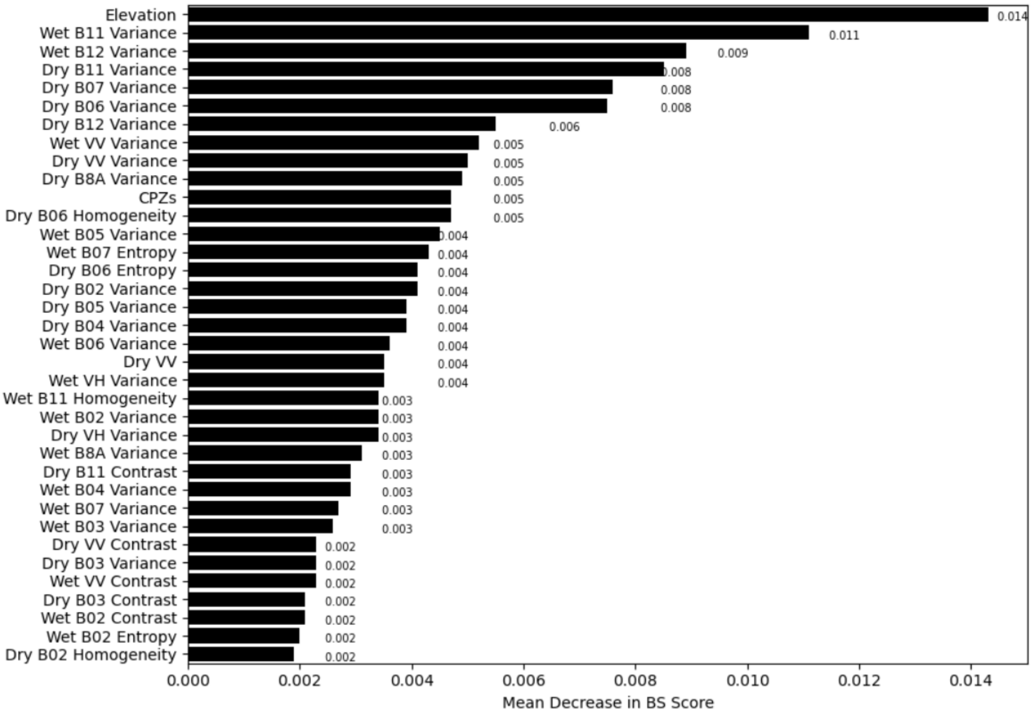

Figure 16 Feature Importance: Mean Decrease in Error

5.4. Estimating AFA fractions at 30m

The fitted RF classification model has been used to predict the probability of AFA per pixel. The derived probability has been calculated by dividing the number of trees with a positive prediction by the total number of trees' prediction or also called 'Class Membership Probabilities.' The model performance has been tested on two individual data set, one is a testing dataset which is based on manual digitization of AFA area on PS images through visual interpretation, and the second one is the validation dataset, which is based on the digitized ground boundary of AFA present in 2017-2019. As observed in the given confusion matrix for testing and validation dataset (Table 5 &

Table 6), both datasets have a vast difference in the total number of samples because of the time and cost involved in collecting on-ground measurements (validation dataset). Although, both datasets have lower AFA observations comparing to non-AFA observations representing imbalance in both datasets. The classification of the pixels into specific AFA or non-AFA category is based on estimated probabilities as well, in which probabilities of AFA more than 0.5 are classified as AFA and vice versa for non-AFA. These confusion matrices have been further used to calculate ROC AUC and error matrix to test the quality of model for class prediction and, BS and pseudo R^2 have been used to test the quality of model for predicting the probabilities of AFA per pixel.

Table 5 Confusion Matrix for Testing Dataset

	Non-AFA	**AFA**	**Total**
Non AFA	22,818	46	22,864
AFA	328	2439	2767

Table 6 Confusion Matrix for Validation Dataset

	Non-AFA	**AFA**	**Total**
Non AFA	48	0	48
AFA	6	7	13

The ROC AUC on the testing data set was 0.93, and on the validation dataset was 0.76 showing the robustness of the model performing approximately similar with marginal error on both dataset, although due to imbalanced dataset and predicting single class label based ROC AUC based interpretation can be misleading. Table 7 shows the error matrix stating the precision, recall, and f1-score for both testing and validation datasets. Precision shows the total relevance or confidence in the prediction, and recall explains the total correct class prediction out of all specific class samples or completeness of the predictions. Both confidence and completeness for predicting non-AFA are high compared to AFA predictions with 0.99 precision and 1.00 recall rate testing dataset for the non-AFA area. While predicted, AFA has high confidence with 0.98 precision rate on a testing dataset but has more omissions of AFA samples with a 0.88 recall rate. The similar behavior for predicting AFA on the validation dataset can be observed with a 1.00 precision rate and 0.54 recall rate, showing higher confidence in prediction AFA but have a higher fall-out rate of sample points. Although it is necessary to interpret these results with caution as changing the probability threshold of 0.5 for final class label prediction can change the error matrix. It is also important to note that the final results of the research are continuous probabilities map of AFA and not a single class label, for which pseudo R^2 and BS has been used to evaluate the model performance.

Table 7 Error Matrix

	Testing Dataset			**Validation Dataset**		
	Precision	Recall	f1-score	Precision	Recall	f1-score
Non AFA	0.99	1.0	0.99	0.89	1.00	0.94
AFA	0.98	0.88	0.93	1.00	0.54	0.70

The pseudo R^2 for the testing dataset is 0.78, and for validation, the dataset is 0.50. The lower variation explained based pseudo R^2 in mapped probabilities for validation dataset could be because of the small sample size of the validation dataset and limit the interpretation of the result. Moreover, it also questions the robustness of the model for predicting % probabilities in mixel. The stated R^2 values are leveraged by extremes, meaning the model is predicting 0% to 0.5% probabilities for non-AFA and 0.5% to 1% probabilities for AFA. The confidence or error remained in predicting probabilities explained via BS. BS explains mean squared error in the actual vs. predicted probabilities, therefore the lower the error, the better predictions of probabilities can be interpreted. BS with value 1 shows the worst predictions, and 0 shows the perfect predictions, it can also be considered as a cost function where the score penalizes higher weights for the higher difference between actual and predicted probabilities. Here, the BS has been analyzed for positive probability prediction or probabilities of AFA prediction as it is the target output. The BS score on testing data was 0.01, and on the validation dataset was 0.1, indicating the close predictions of probabilities for AFA with the actual probabilities have been achieved on both testing and validation datasets.

To understand the behavior pattern of image features for estimating probabilities of AFA can be described in brief via Partial Dependence Plot (PDP), as shown in Figure 17. The plot explains the relationship of change in probabilities of AFA with the change in mapping predictor or image feature with AFA probabilities. Here only a few distinct variables, and its behavior have been explained for understanding the PDP of all 36 variables used in the model (see Appendix B). Based on Figure 17, it can be inferred that lower elevated (0-200m) or valley areas in the region have lower AFA probabilities compared to the hilly areas (200 – 400m). Meanwhile, AFA probabilities decrease with higher values of

VV band in dry seasons, which is obvious as the higher value of VV bands shows the taller vertical features like trees or forest while lower values indicate bare soil. Not only topographic and polarimetric but also temporal image features, that is, CPZs, indicating an increase in AFA probabilities with higher intensity CPZs. There were a total of 15 CPZs have been used, out of which only three zones have higher cropping intensity, that is above 30%, only these zones have explained increased probabilities of AFA at 30m resolution. As shown in Figure 13, the forest area or area with homogenous pattern have lower variance compared to fields or urban area. Similar implications can be derived based on PDP, where dry and wet SWIR (B11) variance shows a decrease in probabilities and slowly linear increase in probabilities with increasing variance. Also, it is important to observe that there is a sudden hike showing increasing in AFA probabilities by increasing the variance in wet seasons B11 variance comparing to dry seasons due to the difference between bare soil and crop area present on AFA.

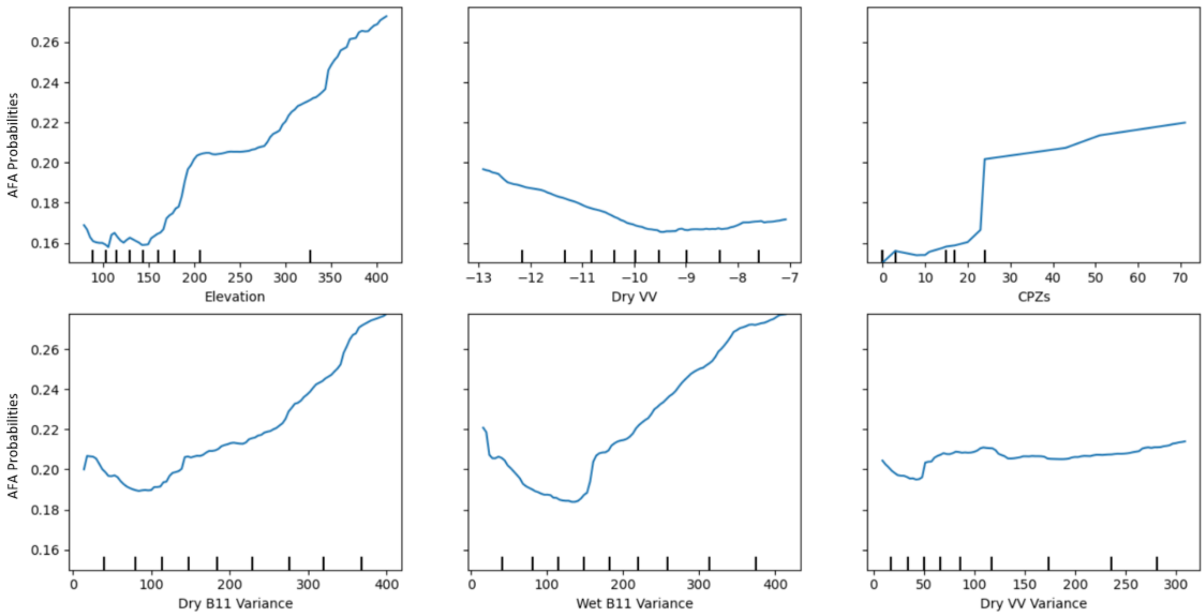

Figure 17 Partial Dependence Plots

One of the main reasons could be the terrain characteristic of area and farming practices followed on hilly areas in the Eastern region. The main reason could be the arable fields' characteristics and similarity in temporal and spectral characteristics with natural vegetation. Figure 18 shows the AFA probabilities at 30m resolution (for more example, see Appendix C). The total AFA area (maize, cassava, rice) in Eastern region was reported by Ministry of Food and Agriculture (MoFA) in 2016 was 2742 km^2 area while considering all the % estimated probabilities per pixel of AFA in this study the total estimated AFA is 10,000 km^2 (considering probabilities more than 0.5). The overall model shows the overestimation of the cropped area; however, this result should be interpreted with caution as even lower probabilities have been considered in reported statistics.

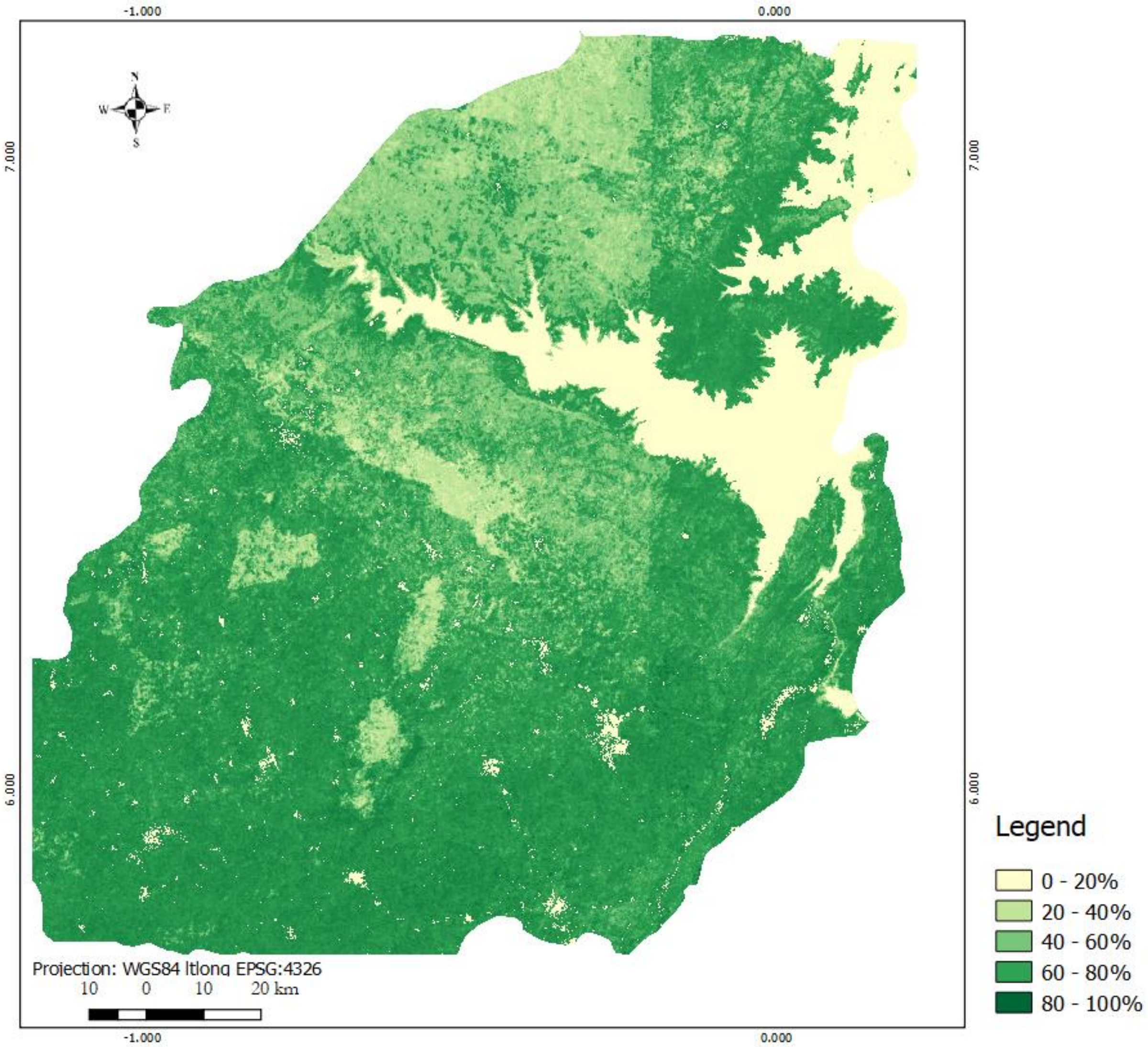

Figure 18 AFA probability map at 30m

Considering the mapped probabilities map (Figure 18), Figure 19 shows the example of optical (RE B6) and radar (VV) variance texture features of the dry and wet season for mapping probabilities. As observed homogenous areas like water have lower variance, highly cropped areas have moderate variance in texture, and heterogeneous areas near water boundaries with mixed vegetation and bare areas have higher variance in both optical and radar texture features. Zooming into only AFA or cropped areas, the radar variance texture feature shows a lower increase or change in the wet season compared to the dry season than optical texture features, one of the main reason can be the sensitivity of VV radar backscatter to water content in vegetation and optical height of the crop. For example, if crop height can fluctuate with the increase or decrease water content over the wet season resulting in sometimes marginal changes in VV backscatter. Although, optical RE bands have sensitivity towards plant chlorophyll content, which keeps increasing over growing season with increasing photosynthetic activities. Because of it, the higher discrimination between wet and dry optical variance features can be observed compared to marginal discrimination of radar variance features.

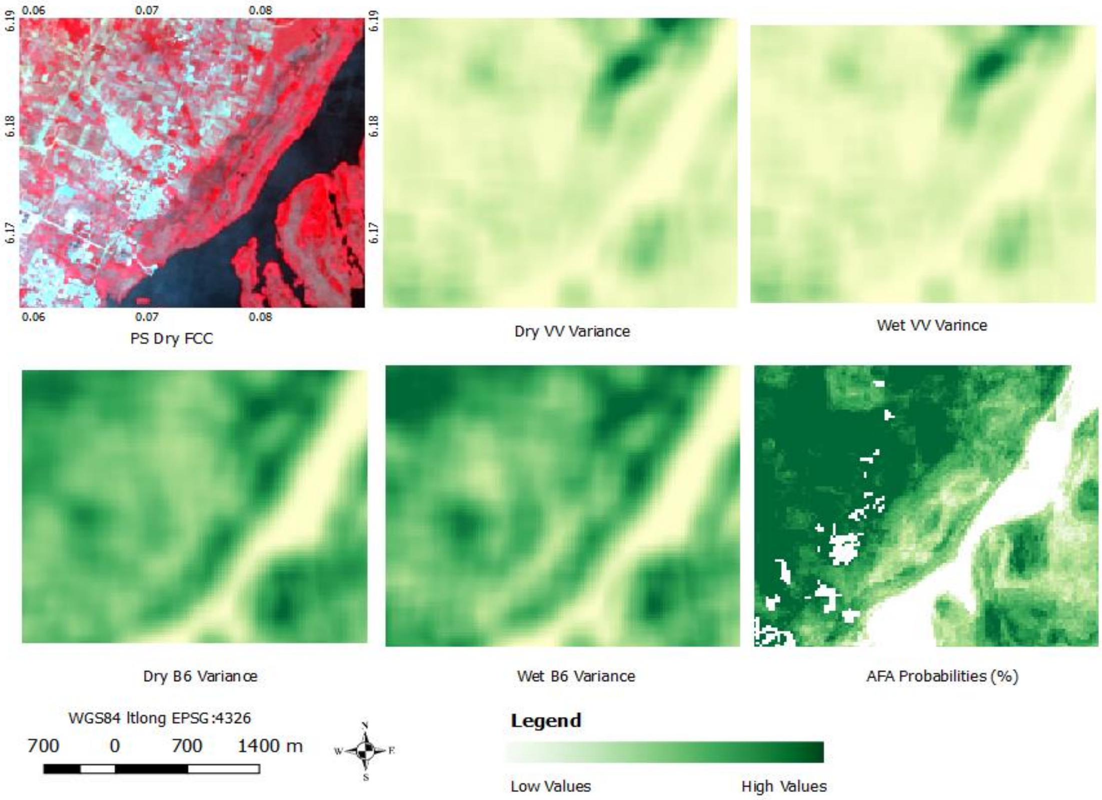

Figure 19 Texture Features and Mapped Probabilities

6. DISCUSSION

In this research effort of mapping, AFA has carried out in an intense cloudy region with a heterogeneous agricultural landscape of West Africa with the elegant machine learning modeling (RF) technique. The research comprehensively studies freely available satellite-based temporal, spectral, polarimetric, and topographic image features (total 137 features) to identify physical factors explaining AFA distribution as the main aim of the research. These physical image features reflect insights into the ongoing farming activities or other land use changed induced actions in the imageries with moderate spatial and temporal resolution images (S1&S2). Out of these image features, topography based elevation has been found very useful in explaining the AFA distribution at the large scale or landscape level which is also inclined with previous findings (Husak et al., 2008b; Marshall et al., 2011a). Therefore, it can be implied that topography is the most important image feature in complex terrains. After topography, optical and radar-based texture features have been found important mapping predictors for AFA, implying texture features are more important than spectral, temporal, and polarimetric features inclined with findings by Vintrou et al., (2012). Regardless of cloud-free measurements captured by S1, long-term median composite (3-years) of S2 optical texture image features, specially SWIR and RE bands, have explained more variation compared to radar texture features in complex agriculture landscape. However, the combined use of optical and radar texture features is important, and radar texture features do improve the model performance by a marginal increase inaccuracy. Similar observations have been made by Van Tricht et al., (2018) and Yin et al., (2020). Followed by texture features, temporal and polarimetric image features are identified as important mapping predictors as well for AFA mapping. While, none of the spectral features has been found important compared to texture, topographic, temporal, and polarimetric image feature.

Mapped probabilities do align with the overall CPZs and rainfall distribution, showing lower (0-30%) or moderate probabilities (40-50%) in the northern area (drier climate) and higher probabilities in southern areas. Although it also has an exception like a lower area in the southern part, it has CPZs with higher cropping intensity than a highly elevated (>550m) area. This consideration is also included by the model and can be seen in the final crop probabilities. In general, the area has lots of hills rather than steeper mountains, as you can see in Figure 14, the Afarm plains (north part) are relatively flat (elevation) than the middle areas near Lake Volta which are highly elevated (>550m elevation) and the southern areas have lots of hills (0-450m elevation). Though the area has a higher variation in elevation, it does not have much steeper topography, as shown in Figure 14. The steepest area is in the between south and north Easterner region with the highest elevation while in the south and Afarm plains, the area has very little steepness (0-10%). Moreover, based on the on-ground observations, these higher elevated and stepper area has rocks while other hilly areas in the south and Afarm plains are with red or clay soil, making low altitude or hilly area more suitable for farming, in this study only topography has been considered and found most important mapping predictor in complex topographical agriculture landscape. It explains the lower probabilities of the area having arable fields in lower altitude drier areas (here: Afarm plains, areas far from lake Volta) due to rainfall intensity (lower), temperature (higher), and lack of irrigation facilities. On the other hand, very high altitude areas (here: >550m) also have lower probabilities of AFA mainly because of high steepness, rocky soil, and high temperature, which are well explained by elevation image feature. The area with moderate elevation (here: 0-400m) has higher probabilities of AFA, which is also one of the reasons for explaining elevation as more discriminant features compared to the slope. The low steeped area with (majority slope: 0-10%) or hills does not help to determine the probability of the location being AFA while the position of the location (higher elevated or lower elevated) does. Elevation does not only helped to capture AFA on the regional scale but also on a local scale showing higher probabilities of AFA on hilly area comparing to valley area (near Lake Volta in Afarm plains), as valley area get flooded in the heavy monsoon season due to which it has lower suitability for farming practices.

They are considering the combined group 2 (optical texture features) & group 3 (radar texture features) as per Table 4 of the discriminant image features helps to improve mapping AFA with a 0.05-0.06% decrease in BS error. It shows that consideration of neighborhood pixel intensity is more useful than spectral rationing or spectral image features in heterogenous complex landscapes by considering the geography of the area. Within the texture features as well, optical (RE & SWIR) S2 based texture features have outperformed the radar S1 based texture features. However, radar texture features are added value for mapping AFA explaining a 0.01% decrease in BS error. It does not imply that radar texture features are not important, but optical texture features explain unique variation by individual band compared to radar texture features. One of the main reasons for it is the sensitivity of radar backscatter towards topography. As topography has been included as an individual mapping predictor, it explains the majority of the variation in AFA distribution. Second, due to viewing geometry as well, foreshortened masked S1 radar images are unable to capture the distribution of AFA in high elevated areas or stepper areas.

Moreover, it is sensitive towards moisture and vegetation water content, which explains the biophysical parameters (height, biomass) or crop conditions during the growing season. The frequent fluctuations in rainfall and temperature over and within the dry and wet seasons affect crop conditions heavily, which reflects lower variation in the median composite of radar image features of the dry and wet season. On the other hand, optical (SWIR & RE) images are sensitive to plant pigment (chlorophyll, nitrogen) content, which keeps increasing during the growing season, which is also less sensitive to biophysical conditions of crops.

Considering the S2 based optical texture features, narrow spectral bands like SWIR (B11, B12), RE (B6, B7) and NIR (B8A) based texture features are more important than other bands (VIS) due to sensitivity of SWIR to the moisture content in soil and vegetation, the sensitivity of RE & NIR to the plant chlorophyll and nitrogen content into the plant, also observed by Yin et al., (2020). Not only the biochemical structure of vegetation but also the difference in physical structure between AFA and tree crops has been captured via radar-based VV band texture features, which capture the difference in the height of the vegetation, also observed by Harfenmeister, Spengler, & Weltzien (2019). Within the texture features only, variance texture features have more predicting power compared to homogeneity, contrast, entropy, and dissimilarity as the variance of specific pixel window (here: 11x11) reduces the complexity or randomness of the pixels observations via preserving edges and geography of the surface features, which is also found in relative studies (Braun, Lang, & Hochschild, 2016). Based on this study and visual interpretation, it is suggested to implement the calculation of texture features using raw backscatter values of S1 and surface reflectance values of S2 bands without any pre-smoothing or speckle filtering at 30m helps to capture the finer geographic features like small and sparse arable fields. It is also important to note that the challenge of extreme cloud cover optical images have been addressed via the median composite of the images over three years (2017-2019), which indirectly strengthens the capabilities of S2 texture images to capture vegetation difference in dry as well as the wet season.

After topographic and texture features, CPZs temporal image feature shows a 0.05% decreased in BS error. CPZs based on long-term MODIS NDVI temporal profiles show regional level variation in AFA probabilities by capturing the difference in the distribution of AFA. This depicts that CPZs with higher probabilities of AFA helps to predict AFA with better compared to CPZs with lower probabilities of AFA. Incorporating, lower spatial resolution CPZs with a moderate spatial resolution (30m) topographic and texture features explain the regional and local variation of AFA distribution well. Although it is necessary to interpret the results as in this study consciously, CPZs are derived from 2003 to the 2009 year data assuming that not any drastic landcover change happened. The minor changes in results can be expected using the latest MODIS data.

In a way, texture-based dry VV variance and wet VV variance shows better prediction capabilities than polarimetric dry VV image feature (0.04% decrease in BS error) considering the neighborhood pattern of pixels reduces the complexity of fragmented agricultural landscapes. However, the polarimetric dry VV image feature shows more discrimination in AFA distribution than wet VV image features due to similarity in biophysical parameters of arable fields and natural vegetation during the wet season. Countries like Ghana, where rain-fed agriculture is prominent, and farm mechanization is less adopted, S1 based radar measurement in wet season may show similar stress or health condition (moisture content-based) and similar height between natural vegetation and arable crops due to dependency of rainfall intensity and radar backscatter sensitivity toward water content. Besides, in dry season difference in measurements due to crop height of S1 backscatter between vegetated (natural vegetation) and non-cropped (bare soil or plowed fields) area are captured.

Not only identifying relevant image features and its predicting power for mapping AFA are studied but also developing an elegant mapping approach that is easy to adopt for mapping AFA in complex agriculture landscape is one of the endeavors tried out in the research. West African countries often have extreme, and longer rainfall intensity showing due to which there is an extreme cloud cover can be observed, which challenges the use of optical images. Therefore, in this study, the median composite of three years (2017-2019) of images has been used to create cloud-free optical S2 images. A similar methodology applies to radar S1 images, which smooth out the backscatter values over the period showing less randomness in the pixels. Using this simple approach, creating cloud-free images is easy, and it is necessary as the majority of the important image features are S2 SWIR and RE based texture features.

Since the target class is AFA, capturing seasonal changes is very important to differentiate AFA with other vegetation like tree crops and natural vegetation, which have been introduced via simple prototyping of agroecological zone-specific dry and wet season using moving average method. There are few studies which have used single dry and wet season period fixed for the whole region to map agriculture area, although in this study reveals that the vegetation seasons do changes across the region mainly because of farming practices, farm mechanization, and rainfall distribution and, therefore it is important to consider agroecological zone-specific seasons to synthesis moderate spatial resolution (30m) based dry and wet season image feature. It is important to note that, in this study, the dry and wet annual seasons have been characterized based on long-term higher temporal MODIS based averaged NDVI profiles from 2003 to 2009, assuming that there are no significant changes in farming practices (sowing & harvesting) in the region. This assumption has also tested with on-ground surveys and interviews with farmers and agriculture officers in 2020.

The mapping probabilities of AFA in this study is carried out by the probabilistic RF algorithm as it is easy to implement and easy to understand. The study uses a dummy RF algorithm trained on BS loss function to identify the mean decrease in error rate by individual mapping predictor. Based on the resulted 36 important image features, It is implied that the RF is very efficient in identifying the discriminant image features in high and correlated feature space. However, mapped AFA probabilities, in general, tend to overestimate the AFA per pixels due to lower confidence in prediction for AFA than the non-AFA. The major reason behind that could be the lower number of samples for AFA compared to non-AFA, and also RF algorithms are sensitive to sample design (Belgiu & Drăgu, 2016). Though it is easy to adopt, it may require higher computational resources and larger feature space or sample size. Also, to mapping AFA, the trained model performs well on hold-out or testing data but does not perform well on the validation dataset (explained by lower R^2 value for validation dataset). Also, in terms of the testing dataset, mapped probabilities are leveraged for extreme values (0 and 1 value), meaning not exact predictions like 0 – 0.3 for values 0 and 0.8 to 1 for value 1 are made. A similar pattern can also be observed on the validation dataset. This model performance implies that the trained model is not stable and is not transferrable; in other words, not robust to a great extent. The possible reasons behind that can be RF does not support the quasibinomial distribution based learning mechanism where actual data follows beta distribution (continuous 0 to 1 values) of AFA. It can be improved by a beta distribution based RF model or further possible reasons like over smoothing due to the cubic convolution resampling technique, criteria used (binomial) for RF that should be improved. Additionally, hyper-parameter tuning and localization of the regional model can also be used for marginal improvements.

In this study, the random sampling combined with stratified sampling per CPZs has been adopted to manually digitized arable fields based on seasonal PS images. The sample size included in the research is huge (93,000 approx. samples) yet biased (only 17,000 pixels have % of AFA) with an efficient approach to derive mapped probabilities per sample polygon grid from digitized labels. However, the imbalance in sample size between classes (non-AFA and AFA) has a huge difference, which can be addressed by including only AFA samples and beta distribution based RF or by increasing intensive sampling in the AFA area compared to non-AFA which may also help to improve confidence and completeness (precision and recall) for predicting probabilities for AFA.

7. CONCLUSION

This study focuses on finding the potential of open-source S1 and S2 data via these long-term median composites to map the AFA area. And it is found out that due to the amount of noise present in the data S1 data and complex geography of the landscape shows fewer prediction capabilities than S2 based SWIR and RE channels. Among possible image features, topographic and texture features are essential for mapping AFA in complex terrain and fragmented agricultural landscape. Although, it does have shown discriminant power to map AFA. The study also addresses the challenge with the addition of identifying relevant image features which are capturing the accurate seasonal changes by introducing the agro-ecological zone-specific seasons, cloud cover by considering the median of the image composite over three year periods of time, spectral unmixing of the pixels by explaining AFA probabilities per pixel using multi-source image features. Additionally, the RF algorithm is efficient in mapping AFA by capturing the non-linearity in the data and identifying discriminant image features. It can also be used for regional level mapping and modify easily to develop an automized mapping system. However, important considerations like resampling and splitting criteria are necessary to improve the robustness of the model to map % of probabilities of AFA. On border terms, the location-specific probabilities of the AFA map can be a valuable input to the other modeling application like hydrological, agriculture monitoring, or can be used as a based map for area frame sampling at the regional level. The developed methodology and the end product are easy to derive; therefore, it can be used by the local African government or NGO's.

LIST OF REFERENCES

Abdikan, S., Sekertekin, A., Ustunern, M., Balik Sanli, F., & Nasirzadehdizaji, R. (2018). Backscatter analysis using multi-temporal Sentinel-1 SAR data for Crop growth of Maize in Konya Basin, Turkey. *International Archives of the Photogrammetry, Remote Sensing and Spatial Information Sciences - ISPRS Archives*, *42*(3), 9–13. https://doi.org/10.5194/isprs-archives-XLII-3-9-2018

Ali, A. (2014). *HYPER-TEMPORAL REMOTE SENSING FOR LAND COVER MAPPING AND MONITORING*. Retrieved from https://webapps.itc.utwente.nl/librarywww/papers_2014/phd/amjadali.pdf

Ali, A., de Bie, C. A. J. M., & Skidmore, A. K. (2013). Detecting long-duration cloud contamination in hyper-temporal NDVI imagery. *International Journal of Applied Earth Observation and Geoinformation*, *24*, 22–31. https://doi.org/10.1016/J.JAG.2013.02.001

Ali, A., de Bie, C. A. J. M., Skidmore, A. K., Scarrott, R. G., Hamad, A., Venus, V., & Lymberakis, P. (2013). Mapping land cover gradients through analysis of hyper-temporal NDVI imagery. *International Journal of Applied Earth Observation and Geoinformation*, *23*, 301–312. https://doi.org/10.1016/J.JAG.2012.10.001

Atzberger, C. (2013). Advances in remote sensing of agriculture: Context description, existing operational monitoring systems and major information needs. *Remote Sensing*, *5*(2), 949–981. https://doi.org/10.3390/rs5020949

Baidu, M., Amekudzi, L. K., Aryee, J., & Annor, T. (2017). Assessment of Long-Term Spatio-Temporal Rainfall Variability over Ghana using Wavelet Analysis. *Climate*, *5*(2), 30. https://doi.org/10.3390/cli5020030

Belgiu, M., & Drăgu, L. (2016). Random forest in remote sensing: A review of applications and future directions. *ISPRS Journal of Photogrammetry and Remote Sensing*, *114*, 24–31. https://doi.org/10.1016/j.isprsjprs.2016.01.011

Biau, G. (2012). Analysis of a random forests model. *Journal of Machine Learning Research*, *13*, 1063–1095.

Blaes, X., Vanhalle, L., & Defourny, P. (2005). Efficiency of crop identification based on optical and SAR image time series. *Remote Sensing of Environment*, *96*(3–4), 352–365. https://doi.org/10.1016/J.RSE.2005.03.010

Braun, A., Lang, S., & Hochschild, V. (2016). Impact of Refugee Camps on Their Environment A Case Study Using Multi-Temporal SAR Data. *Journal of Geography, Environment and Earth Science International*, *4*(2), 1–17. https://doi.org/10.9734/jgeesi/2016/22392

Breiman, L. (2001). Random forests. *Machine Learning*, *45*(1), 5–32. https://doi.org/10.1023/A:1010933404324

Brier, G. W. (1950). VERIFICATION OF FORECASTS EXPRESSED IN TERMS OF PROBABILITY. *Http://Dx.Doi.Org/10.1175/1520-0493(1950)078<0001:VOFEIT>2.0.CO;2*. https://doi.org/10.1175/1520-0493(1950)078<0001:VOFEIT>2.0.CO;2

Brown, M. E., Funk, C. C., Galu, G., & Choularton, R. (2007). Earlier famine warning possible using remote sensing and models. *Eos, Transactions American Geophysical Union*, *88*(39), 381–382. https://doi.org/10.1029/2007EO390001

Brownlee, J. (2018). A Gentle Introduction to Probability Scoring Methods in Python. Retrieved May 27, 2020, from https://machinelearningmastery.com/how-to-score-probability-predictions-in-python/

Chen, C., & Liaw, A. (2004). *Using Random Forest to Learn Imbalanced Data*.

Clausi, D. A., & Zhao, Y. (2002). Rapid extraction of image texture by co-occurrence using a hybrid data structure. *Computers and Geosciences*, *28*(6), 763–774. https://doi.org/10.1016/S0098-3004(01)00108-X

Clevers, J. G. P. W., & Gitelson, A. A. (2013). Remote estimation of crop and grass chlorophyll and nitrogen content using red-edge bands on sentinel-2 and-3. *International Journal of Applied Earth Observation and Geoinformation*, *23*(1), 344–351. https://doi.org/10.1016/j.jag.2012.10.008

Connolly-Boutin, L., & Smit, B. (2016). Climate change, food security, and livelihoods in sub-Saharan Africa. *Regional Environmental Change*, *16*(2), 385–399. https://doi.org/10.1007/s10113-015-0761-x

Coulston, J. W., Moisen, G. G., Wilson, B. T., Finco, M. V., Cohen, W. B., & Brewer, C. K. (2012). Modeling percent tree canopy cover: A pilot study. *Photogrammetric Engineering and Remote Sensing*, *78*(7), 715–727. https://doi.org/10.14358/PERS.78.7.715

Crespin-Boucaud, A., Lebourgeois, V., Lo Seen, D., Castets, M., & Bégué, A. (2020). AGRICULTURALLY CONSISTENT MAPPING of SMALLHOLDER FARMING SYSTEMS USING REMOTE SENSING and SPATIAL MODELLING. In *International Archives of the*

Photogrammetry, Remote Sensing and Spatial Information Sciences - ISPRS Archives (Vol. 42, pp. 35–42). International Society for Photogrammetry and Remote Sensing. https://doi.org/10.5194/isprs-archives-XLII-3-W11-35-2020

Cui, Y., Sun, H., Wang, G., Li, C., & Xu, X. (2019). A probability-based spectral unmixing analysis for mapping percentage vegetation cover of arid and semi-arid areas. *Remote Sensing*, *11*(24). https://doi.org/10.3390/rs11243038

Debats, S. R., Luo, D., Estes, L. D., Fuchs, T. J., & Caylor, K. K. (2016a). A generalized computer vision approach to mapping crop fields in heterogeneous agricultural landscapes. *Remote Sensing of Environment*, *179*, 210–221. https://doi.org/10.1016/j.rse.2016.03.010

Debats, S. R., Luo, D., Estes, L. D., Fuchs, T. J., & Caylor, K. K. (2016b). Remote Sensing of Environment A generalized computer vision approach to mapping crop fi elds in heterogeneous agricultural landscapes. *Remote Sensing of Environment*, *179*, 210–221. https://doi.org/10.1016/j.rse.2016.03.010

Enderle, D. I., & Weih, R. C. J. (2005). *Integrating Supervised and Unsupervised Classification Methods to Develop a More Accurate Land Cover Classification. Journal of the Arkansas Academy of Science* (Vol. 59). Retrieved from http://scholarworks.uark.edu/jaashttp://scholarworks.uark.edu/jaas/vol59/iss1/10

ESA. (2020). User Guides - Sentinel-1 SAR - Geophysical Measurement - Sentinel Online. Retrieved June 17, 2020, from https://sentinel.esa.int/web/sentinel/user-guides/sentinel-1-sar/product-overview/geophysical-measurements

Escadafal, R., Girard, M. C., & Courault, D. (1989). Munsell soil color and soil reflectance in the visible spectral bands of landsat MSS and TM data. *Remote Sensing of Environment*, *27*(1), 37–46. https://doi.org/10.1016/0034-4257(89)90035-7

Estes, L.D., McRitchie, D., Choi, J., Debats, S., Evans, T., Guthe, W., … Caylor, K. K. (2016). A platform for crowdsourcing the creation of representative, accurate landcover maps. *Environmental Modelling & Software*, *80*, 41–53. https://doi.org/10.1016/J.ENVSOFT.2016.01.011

Estes, Lyndon D;, D, M., J, C., SR, D., T, E., W, G., … K, C. (2015). DIYlandcover: Crowdsourcing the creation of systematic, accurate landcover maps. https://doi.org/10.7287/PEERJ.PREPRINTS.1030V1

FAO, IFAD, UNICEF, W. and W. 2018. (2018). *The State of Food Security and Nutrition in the World 2018. Building climate resilience for food security and nutrition. Rome, FAO. Licence: CC BY-NC-SA 3.0 IGO. Building climate resilience for food security and nutrition.* https://doi.org/10.1093/cjres/rst006

FAO. (2003). *World agriculture: towards 2015/2030.* Retrieved from www.earthscan.co.uk

Fernández-Manso, A., Fernández-Manso, O., & Quintano, C. (2016). SENTINEL-2A red-edge spectral indices suitability for discriminating burn severity. *International Journal of Applied Earth Observation and Geoinformation*, *50*, 170–175. https://doi.org/10.1016/j.jag.2016.03.005

Gao, B. C. (1996). NDWI - A normalized difference water index for remote sensing of vegetation liquid water from space. *Remote Sensing of Environment*, *58*(3), 257–266. https://doi.org/10.1016/S0034-4257(96)00067-3

Gebejes, A., Huertas, R., Tremeau, A., Tomic, I., Biswas, P. R., Fraza, C., & Hauta-Kasari, M. (2016). Texture characterization by grey-level co-occurrence matrix from a perceptual approach. In *Final Program and Proceedings - IS and T/SID Color Imaging Conference* (Vol. 0, pp. 271–277). Society for Imaging Science and Technology. https://doi.org/10.2352/ISSN.2169-2629.2017.32.271

Geerken, R., Zaitchik, B., & Evans, J. P. (2005). Classifying rangeland vegetation type and coverage from NDVI time series using Fourier Filtered Cycle Similarity. *International Journal of Remote Sensing*, *26*(24), 5535–5554. https://doi.org/10.1080/01431160500300297

Ghana Statistical Service (GSS). (2019). *Rebased 2013-2018 Annual Gross Domestic Product.* Retrieved from http://www.statsghana.gov.gh/gssmain/storage/img/marqueeupdater/Annual_2013_2018_GDP_April 2019 Edition.pdf

Gitelson, A. A., Gritz, Y., & Merzlyak, M. N. (2003). Relationships between leaf chlorophyll content and spectral reflectance and algorithms for non-destructive chlorophyll assessment in higher plant leaves. *Journal of Plant Physiology*, *160*(3), 271–282. https://doi.org/10.1078/0176-1617-00887

Gregorutti, B., Michel, B., & Saint-Pierre, P. (2017). Correlation and variable importance in random forests. *Statistics and Computing*, *27*(3), 659–678. https://doi.org/10.1007/s11222-016-9646-1

Haack, B., & Bechdol, M. (2000). Integrating multisensor data and RADAR texture measures for land cover mapping. *Computers and Geosciences*, *26*(4), 411–421. https://doi.org/10.1016/S0098-3004(99)00121-1

Hannerz, F., & Lotsch, A. (2008). Assessment of remotely sensed and statistical inventories of African

agricultural fields. *International Journal of Remote Sensing*, *29*(13), 3787–3804. https://doi.org/10.1080/01431160801891762
Haralick, R. M., Dinstein, I., & Shanmugam, K. (1973). Textural Features for Image Classification. *IEEE Transactions on Systems, Man and Cybernetics*, *SMC-3*(6), 610–621. https://doi.org/10.1109/TSMC.1973.4309314
Harfenmeister, K., Spengler, D., & Weltzien, C. (2019). Analyzing temporal and spatial characteristics of crop parameters using Sentinel-1 backscatter data. *Remote Sensing*, *11*(13). https://doi.org/10.3390/rs11131569
Hastie, Trevor, Tibshirani, Robert, Friedman, J. (2009a). *The Elements of Statistical Learning The Elements of Statistical LearningData Mining, Inference, and Prediction, Second Edition*. *Springer series in statistics*. https://doi.org/10.1007/978-0-387-84858-7
Hastie, Trevor, Tibshirani, Robert, Friedman, J. (2009b). *The Elements of Statistical Learning The Elements of Statistical LearningData Mining, Inference, and Prediction, Second Edition*. *Springer series in statistics*. https://doi.org/10.1007/978-0-387-84858-7
Herold, N. D., Haack, B. N., & Solomon, E. (2005). Radar spatial considerations for land cover extraction. *International Journal of Remote Sensing*, *26*(7), 1383–1401. https://doi.org/10.1080/01431160512331337998
Herold, Nathaniel D., Haack, B. N., & Solomon, E. (2004). An evaluation of radar texture for land use/cover extraction in varied landscapes. *International Journal of Applied Earth Observation and Geoinformation*, *5*(2), 113–128. https://doi.org/10.1016/j.jag.2004.01.005
Husak, G. J., Marshall, M. T., Michaelsen, J., Pedreros, D., Funk, C., & Galu, G. (2008a). Crop area estimation using high and medium resolution satellite imagery in areas with complex topography. *Journal of Geophysical Research*, *113*(D14), D14112. https://doi.org/10.1029/2007JD009175
Husak, G. J., Marshall, M. T., Michaelsen, J., Pedreros, D., Funk, C., & Galu, G. (2008b). Crop area estimation using high and medium resolution satellite imagery in areas with complex topography, *113*. https://doi.org/10.1029/2007JD009175
Immitzer, M., Vuolo, F., & Atzberger, C. (2016). First experience with Sentinel-2 data for crop and tree species classifications in central Europe. *Remote Sensing*, *8*(3). https://doi.org/10.3390/rs8030166
Kahubire, E. B. (2002). *SPATIAL DE-AGGREGATION OF CROP AREA STATISTICS USING REMOTE SENSING, GIS AND EXPERT KNOWLEDGE A Case Study of Ghana*. ITC, University of Twente. Retrieved from https://webapps.itc.utwente.nl/librarywww/papers/msc_2002/nrm/kabuhire.pdf
Kakooei, M., Nascetti, A., & Ban, Y. (2018). Sentinel-1 global coverage foreshortening mask extraction: An open source implementation based on google earth engine. *International Geoscience and Remote Sensing Symposium (IGARSS)*, *2018-July*(2), 6836–6839. https://doi.org/10.1109/IGARSS.2018.8519098
Khan, M. R., de Bie, C. A. J. M., van Keulen, H., Smaling, E. M. A., & Real, R. (2010). Disaggregating and mapping crop statistics using hypertemporal remote sensing. *International Journal of Applied Earth Observation and Geoinformation*, *12*(1), 36–46. https://doi.org/10.1016/j.jag.2009.09.010
Kim, H. O., & Yeom, J. M. (2014). Effect of red-edge and texture features for object-based paddy rice crop classification using RapidEye multi-spectral satellite image data. *International Journal of Remote Sensing*, *35*(19), 7046–7068. https://doi.org/10.1080/01431161.2014.965285
Lebourgeois, V., Dupuy, S., Vintrou, É., Ameline, M., Butler, S., & Bégué, A. (2017). A Combined Random Forest and OBIA Classification Scheme for Mapping Smallholder Agriculture at Different Nomenclature Levels Using Multisource Data (Simulated Sentinel-2 Time Series, VHRS and DEM). *Remote Sensing*, *9*(3), 259. https://doi.org/10.3390/rs9030259
Lohou, F., Kergoat, L., Guichard, F., Boone, A., Cappelaere, B., Cohard, J.-M., … Timouk, F. (2014). Atmospheric Chemistry and Physics Surface response to rain events throughout the West African monsoon. *Atmos. Chem. Phys*, *14*, 3883–3898. https://doi.org/10.5194/acp-14-3883-2014
Loosvelt, L., Peters, J., Skriver, H., Lievens, H., Van Coillie, F. M. B., De Baets, B., & Verhoest, N. E. C. (2012). Random Forests as a tool for estimating uncertainty at pixel-level in SAR image classification. *International Journal of Applied Earth Observation and Geoinformation*, *19*(1), 173–184. https://doi.org/10.1016/j.jag.2012.05.011
Marshall, M. T., Husak, G. J., Michaelsen, J., Funk, C., Pedreros, D., & Adoum, A. (2011a). Testing a high-resolution satellite interpretation technique for crop area monitoring in developing countries. *International Journal of Remote Sensing*, *32*(23), 7997–8012. https://doi.org/10.1080/01431161.2010.532168

Marshall, M. T., Husak, G. J., Michaelsen, J., Funk, C., Pedreros, D., & Adoum, A. (2011b). Testing a high-resolution satellite interpretation technique for crop area monitoring in developing countries. *International Journal of Remote Sensing*, *32*(23), 7997–8012. https://doi.org/10.1080/01431161.2010.532168

Ministry of Food and Agriculture. (2011). Agricutlure in Ghana : Facts and Figures (2010), (May), 1–58. Retrieved from https://www.mendeley.com/viewer/?fileId=31e5e7c8-b7a1-d50d-41cd-02ba97ddc30e&documentId=ffb74be1-bd58-3e62-b1db-8231c720737c

Ministry of Food and Agriculture (MoFA). (2017). *Agriclture in Ghana, Facts and Figure (2016)*. Retrieved from http://mofa.gov.gh/site/wp-content/uploads/2018/05/Agric in Ghana F&F 2016_Final.pdf

Mohammed, I. (2019). *MAPPING CROP FIELD PROBABILITIES USING HYPER TEMPORAL AND MULTI SPATIAL REMOTE SENSING IN A FRAGMENTED LANDSCAPE OF*. ITC, University of Twente.

Mohammed, I., Marshall, M., de Bie, K., Estes, L., & Nelson, A. (2020). A blended census and multiscale remote sensing approach to probabilistic cropland mapping in complex landscapes. *ISPRS Journal of Photogrammetry and Remote Sensing*, *161*, 233–245. https://doi.org/10.1016/j.isprsjprs.2020.01.024

Murmu, S., & Biswas, S. (2015). Application of Fuzzy Logic and Neural Network in Crop Classification: A Review. *Aquatic Procedia*, *4*, 1203–1210. https://doi.org/10.1016/J.AQPRO.2015.02.153

Neigh, C. S. R., Carroll, M. L., Wooten, M. R., Mccarty, J. L., Powell, B. F., Husak, G. J., … Hain, C. R. (2018). Remote Sensing of Environment Smallholder crop area mapped with wall-to-wall WorldView sub-meter panchromatic image texture : A test case for Tigray , Ethiopia. *Remote Sensing of Environment*, *212*(June 2017), 8–20. https://doi.org/10.1016/j.rse.2018.04.025

Ouyang, L., Mao, D., Wang, Z., Li, H., Man, W., Jia, M., … Liu, H. (2017). Analysis crops planting structure and yield based on GF-1 and Landsat8 OLI images. *Nongye Gongcheng Xuebao/Transactions of the Chinese Society of Agricultural Engineering*, *33*(11), 147–156. https://doi.org/10.11975/j.issn.1002-6819.2017.11.019

Pan, Y., Hu, T., Zhu, X., Zhang, J., & Wang, X. (2012). Mapping Cropland Distributions Using a Hard and Soft Classification Model. *IEEE Transactions on Geoscience and Remote Sensing*, *50*(11), 4301–4312. https://doi.org/10.1109/TGRS.2012.2193403

Recio, J. A., Hermosilla, T., Ruiz, L. A., & Fernández-Sarría, A. (2010). *ADDITION OF GEOGRAPHIC ANCILLARY DATA FOR UPDATING GEO-SPATIAL DATABASES*. Retrieved from https://pdfs.semanticscholar.org/3e5a/956d002b92fd477ffed352d1952bbb2cdeb1.pdf

Reed, B. C., Brown, J. F., VanderZee, D., Loveland, T. R., Merchant, J. W., & Ohlen, D. O. (1994). Measuring phenological variability from satellite imagery. *Journal of Vegetation Science*, *5*(5), 703–714. https://doi.org/10.2307/3235884

Rogan, J., Chen, D., & Rogan, J. (2004). Remote sensing technology for mapping and monitoring land-cover and land-use change. *Progress in Planning*, *61*, 301–325. https://doi.org/10.1016/S0305-9006(03)00066-7

Sevillano Marco, E., Herrmann, D., Schwab, K., Schweitzer, K., Almengor, R., Berndt, F., … Probeck, M. (2019). Improvement of existing and development of future copernicus land monitoring products-The ECOLASS project. In *International Archives of the Photogrammetry, Remote Sensing and Spatial Information Sciences - ISPRS Archives* (Vol. 42, pp. 201–208). International Society for Photogrammetry and Remote Sensing. https://doi.org/10.5194/isprs-archives-XLII-2-W16-201-2019

Smith, G. M., & Fuller, R. M. (2001). An integrated approach to land cover classification: An example in the Island of Jersey. *International Journal of Remote Sensing*, *22*(16), 3123–3142. https://doi.org/10.1080/01431160152558288

Symeonakis, E., Higginbottom, T. P., Petroulaki, K., & Rabe, A. (2018). Optimisation of savannah land cover characterisation with optical and SAR data. *Remote Sensing*, *10*(4). https://doi.org/10.3390/rs10040499

Tadesse, H. K., & Falconer, A. (2014). Land cover classification and analysis using radar and landsat data in north central Ethiopia. *ASPRS 2014 Annual Conference: Geospatial Power in Our Pockets, Co-Located with Joint Agency Commercial Imagery Evaluation Workshop, JACIE 2014*.

The World Bank. (2017). *Ghana: Agriculture Sector Policy Note*. Retrieved from http://documents.worldbank.org/curated/en/336541505459269020/pdf/119753-PN-P133833-PUBLIC-Ghana-Policy-Note-Ag-Sector-Review.pdf

Tokarczyk, P., Wegner, J. D., Walk, S., & Schindler, K. (2015). Features, color spaces, and boosting: New insights on semantic classification of remote sensing images. *IEEE Transactions on Geoscience and Remote Sensing*, *53*(1), 280–295. https://doi.org/10.1109/TGRS.2014.2321423

Tran, T. V, Julian, J. P., & De Beurs, K. M. (2014). Land Cover Heterogeneity Effects on Sub-Pixel and Per-Pixel Classifications. *ISPRS Int. J. Geo-Inf*, *3*, 540–553. https://doi.org/10.3390/ijgi3020540

Tucker, C. J. (1979). Red and photographic infrared linear combinations for monitoring vegetation. *Remote Sensing of Environment*, *8*(2), 127–150. https://doi.org/10.1016/0034-4257(79)90013-0

Valero, S., Morin, D., Inglada, J., Sepulcre, G., Arias, M., Hagolle, O., … Thenkabail, P. S. (2016). Production of a Dynamic Cropland Mask by Processing Remote Sensing Image Series at High Temporal and Spatial Resolutions. https://doi.org/10.3390/rs8010055

Van Tricht, K., Gobin, A., Gilliams, S., & Piccard, I. (2018). Synergistic Use of Radar Sentinel-1 and Optical Sentinel-2 Imagery for Crop Mapping: A Case Study for Belgium. *Remote Sensing*, *10*(10), 1642. https://doi.org/10.3390/rs10101642

Vancutsem, C., Marinho, E., Kayitakire, F., See, L., & Fritz, S. (2012). Harmonizing and Combining Existing Land Cover/Land Use Datasets for Cropland Area Monitoring at the African Continental Scale. *Remote Sensing*, *5*(1), 19–41. https://doi.org/10.3390/rs5010019

Vintrou, E., Soumaré, M., Bernard, S., Bégué, A., Baron, C., & Lo Seen, D. (2012). Mapping fragmented agricultural systems in the sudano-sahelian environments of Africa using random forest and ensemble metrics of coarse resolution MODIS imagery. *Photogrammetric Engineering and Remote Sensing*, *78*(8), 839–848. https://doi.org/10.14358/PERS.78.8.839

Waldner, F., Fritz, S., Di Gregorio, A., & Defourny, P. (2015). Mapping Priorities to Focus Cropland Mapping Activities: Fitness Assessment of Existing Global, Regional and National Cropland Maps. *Remote Sensing*, *7*(6), 7959–7986. https://doi.org/10.3390/rs70607959

Watkins, B., & Niekerk, A. Van. (2019). Original papers A comparison of object-based image analysis approaches for field boundary delineation using multi-temporal Sentinel-2 imagery. *Computers and Electronics in Agriculture*, *158*(November 2018), 294–302. https://doi.org/10.1016/j.compag.2019.02.009

Worldatlas. (2017). Geography of Ghana, Landforms, Glaciers, Mt. Mckinley - World Atlas. Retrieved October 1, 2019, from https://www.worldatlas.com/webimage/countrys/africa/ghana/ghland.htm

Xiong, J., Thenkabail, P. S., Gumma, M. K., Teluguntla, P., Poehnelt, J., Congalton, R. G., … Thau, D. (2017). Automated cropland mapping of continental Africa using Google Earth Engine cloud computing. *ISPRS Journal of Photogrammetry and Remote Sensing*, *126*, 225–244. https://doi.org/10.1016/J.ISPRSJPRS.2017.01.019

Xiong, J., Thenkabail, P. S., Tilton, J. C., Gumma, M. K., Teluguntla, P., Oliphant, A., … Gorelick, N. (2017). Nominal 30-m cropland extent map of continental Africa by integrating pixel-based and object-based algorithms using Sentinel-2 and Landsat-8 data on google earth engine. *Remote Sensing*, *9*(10), 1–27. https://doi.org/10.3390/rs9101065

Xu, L., Zhang, H., Wang, C., Zhang, B., & Liu, M. (2018). Crop Classification Based on Temporal Information Using Sentinel-1 SAR Time-Series Data. *Remote Sensing*, *11*(1), 53. https://doi.org/10.3390/rs11010053

Yin, L., You, N., Zhang, G., Huang, J., & Dong, J. (2020). Optimizing Feature Selection of Individual Crop Types for Improved Crop Mapping. *Remote Sensing*, *12*(1), 162. https://doi.org/10.3390/rs12010162

Zakeri, H., Yamazaki, F., & Liu, W. (2017). Texture analysis and land cover classification of tehran using polarimetric synthetic aperture radar imagery. *Applied Sciences (Switzerland)*, *7*(5). https://doi.org/10.3390/app7050452

APPENDIX A

Due to the high dimensionality of the data, correlated features have been observed based on the correlation matrix (below image). The first 110 image features are texture features (upper left corner), and from 110 to 124 features are spectral features (lower right corner), among which the high correlation has been identified.

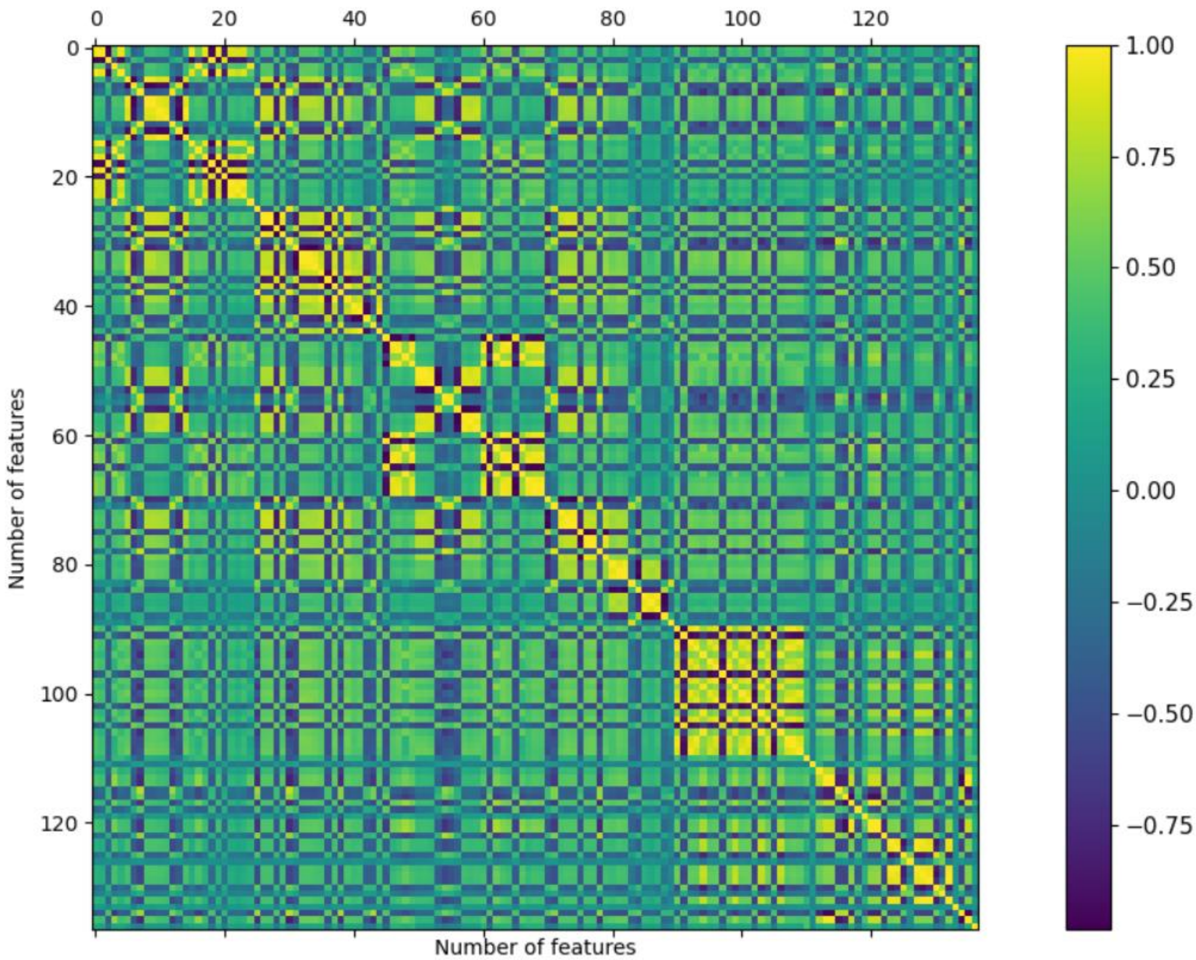

APPENDIX B

Partial Dependence Plot(s) of all relevant image features and mapped AFA.

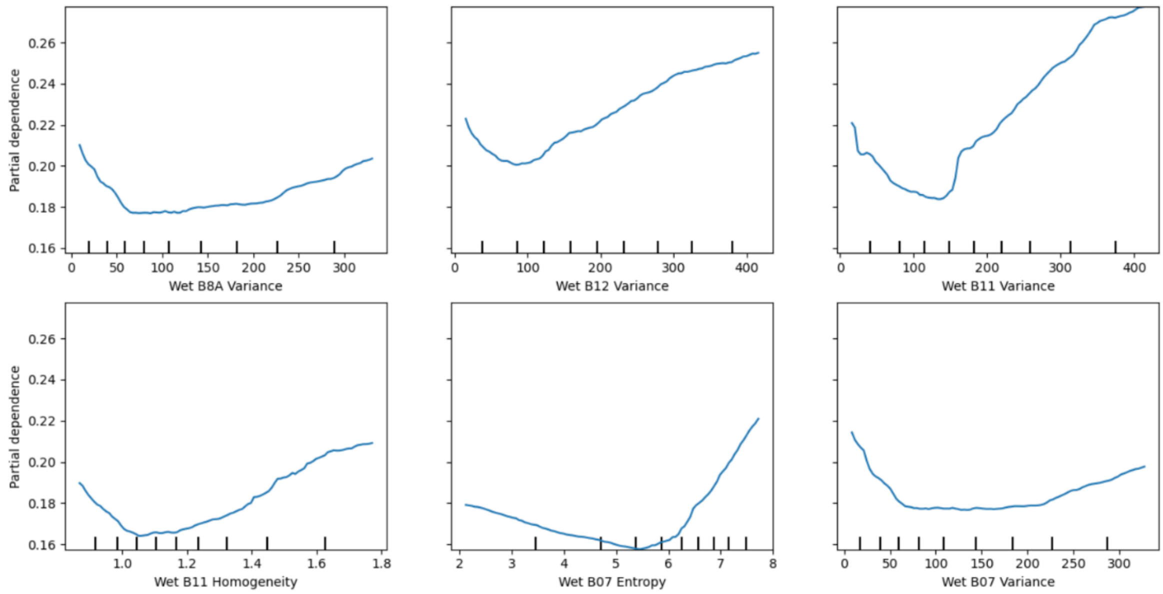

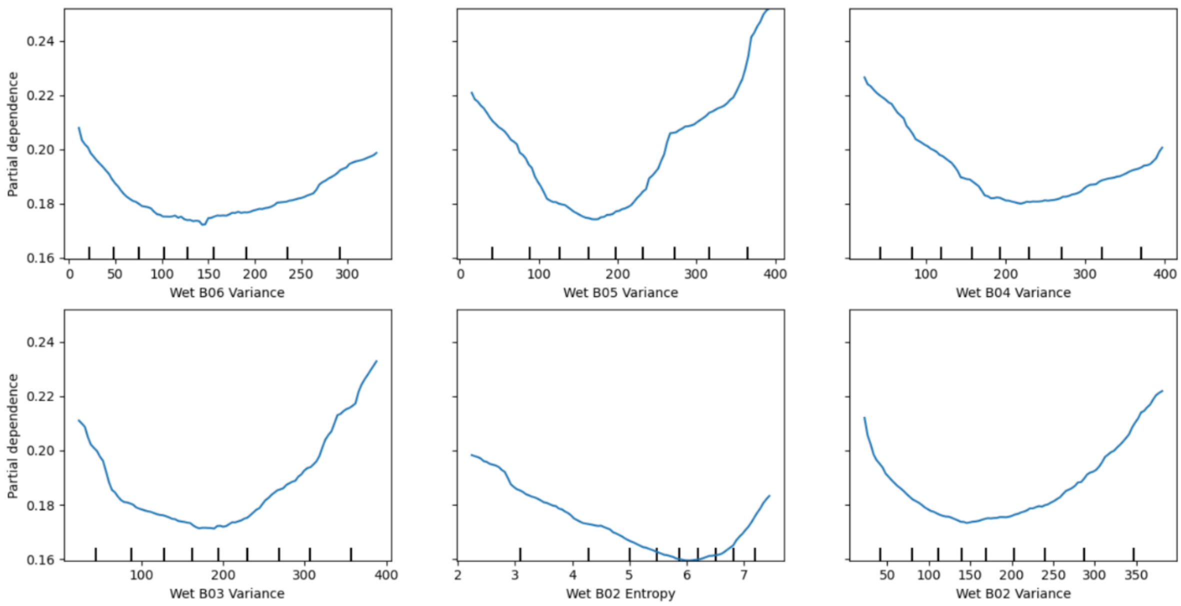

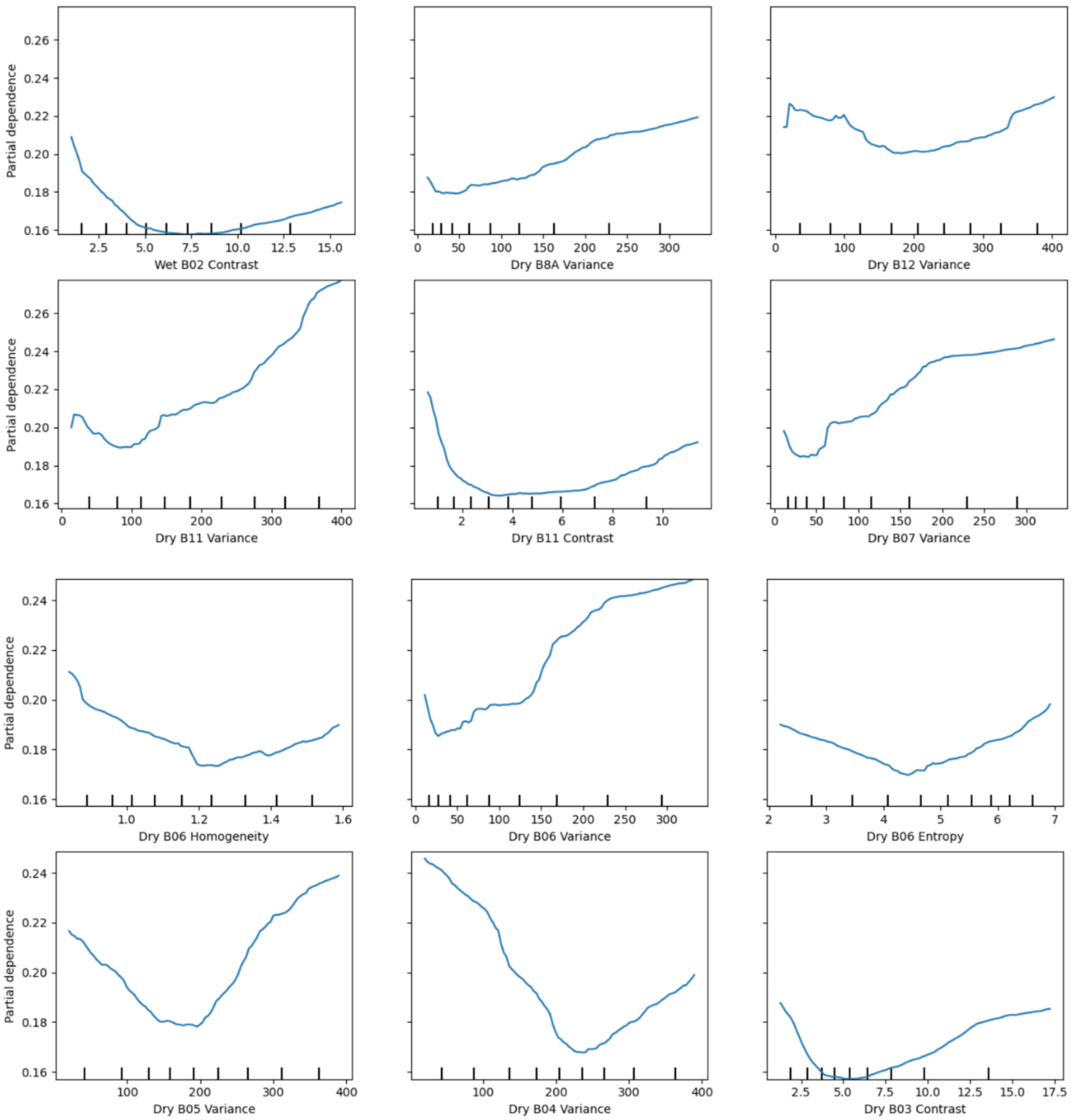

Partial dependence
Wet B02 Contrast
Dry B8A Variance
Dry B12 Variance
Partial dependence
Dry B11 Variance
Dry B11 Contrast
Dry B07 Variance
Partial dependence
Dry B06 Homogeneity
Dry B06 Variance
Dry B06 Entropy
Partial dependence
Dry B05 Variance
Dry B04 Variance
Dry B03 Contrast

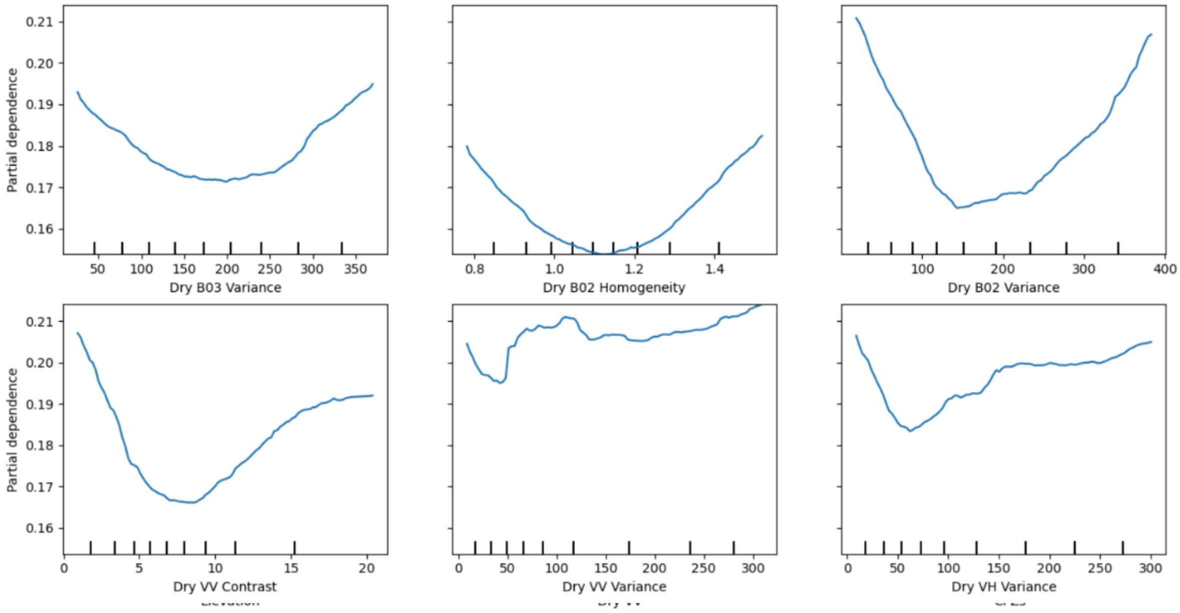
Partial dependence
Dry B03 Variance
Dry B02 Homogeneity
Dry B02 Variance
Dry VV Contrast
Dry VV Variance
Dry VH Variance

APPENDIX C

In this appended, FCC of PS images vs. mapped probabilities at 30m has been shown as various examples. Where darker green color shows higher probabilities and lighter yellow or red color probabilities shows (<0.5) probabilities.